The Astronomical Journal, 135:2496–2525, 2008 June doi:10.1088/0004-6256/135/6/2496

THE EVOLUTION OF THE MULTIPLICITY OF EMBEDDED PROTOSTARS. I. SAMPLE PROPERTIES AND BINARY DETECTIONS*

Michael S. Connelley[1], Bo Reipurth[2], and Alan T. Tokunaga[3]
[1] NASA Ames Research Center, MS 245-6, Moffett Field, CA 94035, USA; michael.s.connelley@nasa.gov
[2] University of Hawai'i Institute for Astronomy, 640 N. Aohoku Pl., Hilo HI 96720, USA; reipurth@ifa.hawaii.edu
[3] University of Hawai'i Institute for Astronomy, 2680 Woodlawn Dr., Honolulu, HI 96822, USA; tokunaga@ifa.hawaii.edu
Received 2007 September 22; accepted 2008 March 3; published 2008 May 15

ABSTRACT

We present the observational results of a near-infrared survey of a large sample of Class I protostars designed to determine the Class I binary separation distribution from ∼100 AU to ∼5000 AU. We have selected targets from a new sample of 267 nearby candidate Class I objects. This sample is well understood, consists of mostly Class I young stellar objects (YSOs) within 1 kpc, has targets selected from the whole sky, and is not biased by previous studies of star formation. We have observed 189 Class I YSOs north of $\delta = -40^\circ$ at the H, K, and L' bands, with a median angular resolution of 0$''$.33 at L'. We determine our detection limit for close binary companions by observing artificial binaries. We choose a contrast limit and an outer detection limit to minimize contamination and to ensure that a candidate companion is gravitationally bound. Our survey uses observations at the L' rather than the K band for the detection of binary companions since there is less scattered light and better seeing at L'. This paper presents the positions of our targets, the near-IR photometry of sources detected in our fields at L', as well as the observed properties of the 89 detected companions (73 of which are newly discovered). Although we have chosen contrast and separation limits to minimize contamination, we expect that there are about six stars identified as binary companions that are due to contamination. Finder charts at L' for each field are shown to facilitate future studies of these objects.

Key words: binaries: general – infrared: stars – stars: formation – stars: statistics

Online-only material: machine-readable tables

1. INTRODUCTION

Ever since it was demonstrated that there must be physically bound pairs of stars and star clusters (Mitchell 1767), the question of binary star formation has been an unsolved problem in astronomy. Duquennoy & Mayor (1991) reported that the solar-type main-sequence binary frequency[4] is 50% ± 5.5% for stars with periods from less than a day to over 10 million years without completeness correction, and 61% after completeness correction. Based on the statistics of the main-sequence binary population, Larson (2001) concluded that "stars seldom if ever form in isolation."

The binary frequency of T Tauri stars has also been carefully studied because they are young, there are a large number of them, and they are optically visible. Reipurth & Zinnecker (1993) conducted an optical survey of 238 southern pre-main-sequence stars and found a binary frequency of 16% ± 3% over the range of projected separations from 150 to 1800 AU. More recently, Mathieu et al. (2000) and Patience et al. (2002) tabulated the results of multiplicity surveys among pre-main-sequence stars. Overall, T Tauri stars are found to have roughly twice the binary frequency compared to main-sequence solar-type stars over the separation ranges covered by these studies.

Duchêne et al. (2004) and Haisch et al. (2004) have published results from searches for embedded binary young stellar objects (YSOs) in nearby star-forming regions. Duchêne et al. (2004) found a binary frequency of ∼26% ± 8% in the separation range from 110 AU to 1400 AU in a survey of 63 flat spectrum and Class I YSOs in the Taurus and Ophiuchus clouds. Haisch et al. (2004) observed a similar sample of 76 YSOs in the Perseus, Taurus, Chamaeleon, Ophiuchus, and Serpens clouds, finding a binary frequency of 18% ± 4% in the separation range from 300 AU to 2000 AU. Combining both results, Duchêne et al. (2007) found a total of 19 companions to 119 stars, yielding a binary frequency of 16% ± 4% from 300 to 1400 AU. This is roughly twice the binary frequency of main-sequence stars over the same separation range, and is consistent with the binary frequency of T Tauri stars.

We have performed a major study of the binarity of Class I sources, which we present in this and a companion paper (Connelley et al. 2008, hereafter Paper II). New observations were required to investigate a larger sample spread over a wider range of star-forming regions at higher angular resolution than previous studies. The goal of this paper is to present the sample of Class I YSOs we observed (Section 2) and our observational results (Section 3). We discuss how we identified binaries and minimized contamination through a choice of contrast and separation limits (Section 4). We also include the properties of the binary companions that we found, including binary systems with strong color differences (Section 5) that are analogs to infrared companions to T Tauri stars. In Paper II we present the Class I binary separation distribution using the data presented here. That paper also includes comparisons of the Class I binary separation distribution with the results of previous studies of Class I YSOs and other pre-main-sequence stars, the evolution of the binary separation distribution within the Class I phase, and the dependence of the Class I binary frequency on the star-forming environment.

* The Infrared Telescope Facility is operated by the University of Hawaii under Cooperative Agreement no. NCC 5-538 with the National Aeronautics and Space Administration, Science Mission Directorate, Planetary Astronomy Program. The United Kingdom Infrared Telescope is operated by the Joint Astronomy Centre on behalf of the Science and Technology Facilities Council of the U.K. Based in part on data collected at the Subaru Telescope, which is operated by the National Astronomical Observatory of Japan.

[4] The binary frequency is the total number of companion stars divided by the number of systems.

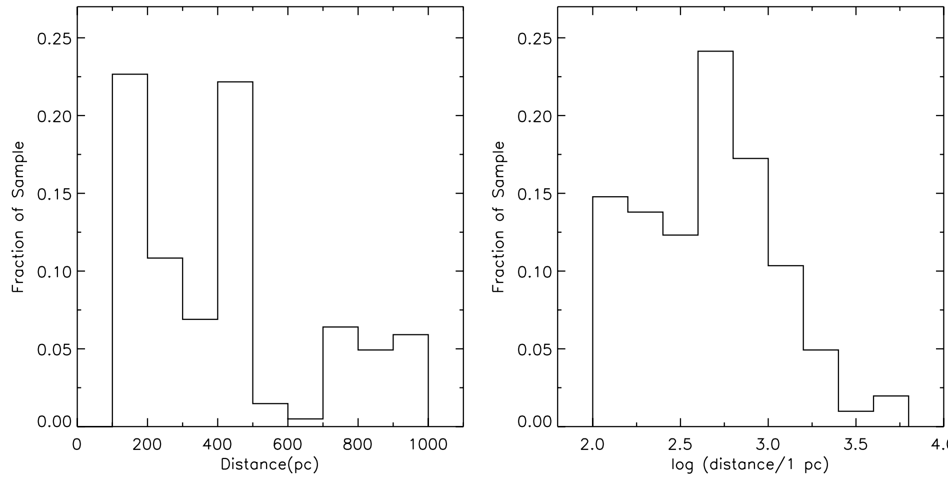

Figure 1. Distance distribution for our sample. The left panel shows the distance distribution for our sample on a linear scale out to a distance of 1 kpc. The right panel presents the same data on a log scale, including targets as far as 6 kpc. Our sample has a median distance of 470 pc and most objects are within 1 kpc.

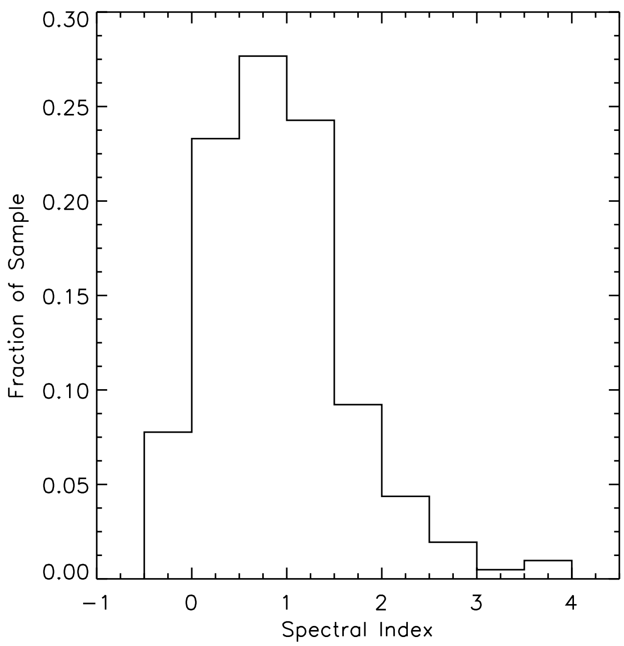

Figure 2. Spectral index distribution. *IRAS* 12 μm to 100 μm fluxes were used to calculate the spectral index, using the method described by Lada (1991). Our sample has a median spectral index distribution of +0.79, thus nearly all of our sources are Class I YSOs.

2. SAMPLE PROPERTIES

We used a new sample of nearby mostly Class I YSOs described in Connelley et al. (2007). Briefly summarized, the sample was selected based on *Infrared Astronomical Satellite* (*IRAS*) colors, coincidence with nearby dark clouds, and coincidence with a red ($H - K \gtrsim 1$) Two Micron All Sky Survey (2MASS) source. Distance estimates, usually to the cloud hosting the protostar, were taken from the literature and are listed in Table 1, along with the source of the distance estimate. The distance distribution (Figure 1) shows that most objects are within 1 kpc, with a median distance of 470 pc. We do not have distance estimates to all of the targets in our sample; however, several targets without distance estimates appear to be associated with well-known clouds. The spectral index distribution (Figure 2) shows that the majority of our targets have a spectral index (Lada 1991) greater than 0, and thus the majority are Class I objects. However, there are a few known T Tauri stars in our sample. For example, FS Tau A was observed since it is a companion to FS Tau B, which is deeply embedded. The sample's spectral index distribution has a median value of +0.79 and a mean value of +0.91. These spectral indices were derived using only *IRAS* fluxes from the Faint Source Catalog if the target is included in that catalog, or the Point Source Catalog if not. We used flux measurements from 12 μm to 100 μm, unless the 12 μm measurement is an upper limit, in which case the spectral index was calculated from 25 μm to 100 μm. Several *IRAS* sources have more than one near-IR counterpart in the *IRAS* beam; thus higher angular resolution far-IR observations may yield different values for the spectral index. The bolometric luminosities of all sources were calculated as described in Connelley et al. (2007). The dearth of sources with $L_{\rm bol} > 100\ L_\odot$ suggests that relatively few of the stars in the sample are high mass stars. This is expected since Connelley et al. (2007) selected against sources associated with H II regions. Similarly, the dearth of sources with $L_{\rm bol} < 0.5\ L_\odot$ shows that it is unlikely that there are many proto-brown dwarfs in the sample.

A goal of the sample selection process was to choose sources across the entire sky, without bias toward well-known star-forming regions. Figure 3 shows the distribution of targets in Galactic coordinates. The shaded area on the right is the part of the sky that is south of $\delta = -40^\circ$. Targets in this region do not rise above two airmasses from Mauna Kea and, aside from two exceptions, were not observed. Our targets are spread across all Galactic longitudes, with clumping in the Taurus/Auriga and Orion star-forming regions. These two regions are both below the Galactic plane and near the Galactic anti-center. Figure 4 shows the arrangement of targets as seen from above the Galactic plane. The targets that are in our sample, including those too far south for us to observe, are listed in Table 1.

3. OBSERVATIONS

3.1. Target Selection

Not all of the targets in the sample were observed in the course of our study. Some of the objects in the sample are T Tauri stars,

Table 1
Source Characteristics

IRAS	Associations	$D(pc)$[a]	L_{bol}	α(J2000)[b]	δ(J2000)[b]	J[c]	H[c]	K_s[c]	α[d]
00182+6223	L1280	4680(4)	366.9	00 20 56.79	+62 40 21.0	15.688	13.982	12.443	1.53
00465+5028	CB6, LBN 613	800(6)	8.8	00 49 24.50	+50 44 43.6	13.822	12.297	11.531	1.01
00494+5617	cluster in NGC 281	2940(21)	9854.4	00 52 23.7[I]	+56 33 45	...	...	...	2.14
01166+6635		249(4)	0.4	01 20 03.93	+66 51 35.9	16.029	14.037	12.606	0.38
02086+7600	L1333	180(5)	0.8	02 13 43.61	+76 15 06.0	13.715	12.254	11.193	0.88
02232+6138	cluster	2040(46)	74578.	02 27 01.0[I]	+61 52 14	...	...	...	1.76
02310+6133	IC 1805	2350(22)	1029.9	02 34 48.79	+61 46 44.5	...	...	13.864	1.64
02511+6023	S190 H II	2000(23)	485.6	02 55 01.99	+60 35 41.7	...	14.827	12.698	1.18
03220+3035	L1448 IRS 1, RNO 13	290(1)	2.0	03 25 09.43	+30 46 21.6	12.546	10.896	9.819	0.02
03225+3034	L1448 IRS 3 RNO 14	290(1)	13.1	03 25 36.47*	+30 45 21.4	13.745	12.363	11.095	1.52
03245+3002	L1455 IRS 1, RNO 15 FIR	260(1)	7.9	03 27 38.83*	+30 13 25.0	...	...	...	1.91
F03258+3105		220(47)	32.3	03 28 59.31	+31 15 48.5	16.490	12.528	10.437	0.59
03260+3111	L1450, SVS 3	290(1)	138.4	03 29 10.38	+31 21 59.2	9.368	7.987	7.173	0.58
03260+3111(W)		290(1)		03 29 07.74	+31 21 57.5	...	13.802	10.428	...
03271+3013	in NGC 1333	290(2)	1.6	03 30 15.16	+30 23 49.4	...	...	14.259	0.86
03301+3057	Barnard 1 IRS	290(2)	3.0	03 33 16.68	+31 07 54.9	...	...	14.208	1.52
03301+3111	Barnard 1	290(2)	4.0	03 33 12.84	+31 21 24.1	12.132	10.155	9.002	0.31
03331+6256		1560(4)	58.2	03 37 28.45	+63 06 31.2	...	...	14.590	0.45
03445+3242	HH 366 VLA 1 Barnard 5 IRS 1 L1471	280(1)	3.8	03 47 41.60	+32 51 43.8	...	14.047	11.214	0.16
03507+3801	HH 462	350(1)	2.5	03 54 06.19	+38 10 42.5	12.474	10.863	10.098	0.22
03580+4053	L1443	none		04 01 24.7[I]	+41 01 48	...	...	...	1.40
04016+2610	L1489 IRS, HH 360	140(1)	3.0	04 04 43.05	+26 18 56.2	12.655	10.861	9.199	0.31
04067+3954	L1459	350(1)	15.1	04 10 08.40	+40 02 24.6	13.767	11.478	9.844	1.17
04073+3800	L1473, HH 463	350(1)	22.6	04 10 41.09	+38 07 54.0	15.339	13.552	10.500	0.07
04108+2803(E)	L1495N IRS	140(1)	0.7	04 13 54.72	+28 11 32.9	16.481	13.376	11.063	−0.15
04113+2758		140(1)	1.1	04 14 26.27	+28 06 03.3	12.475	9.878	7.777	−0.13
04169+2702	L1495, near HH 391	140(1)	0.9	04 19 58.45	+27 09 57.1	16.528	12.554	10.428	0.53
04181+2655(N)	HH392	140(1)		04 21 07.95	+27 02 20.4	13.855	12.062	10.543	1.96
04181+2655		140(2)		04 21 10.39	+27 01 37.3	...	13.783	11.085	...
04181+2655(S)		140(1)		04 21 11.47	+27 01 09.4	16.222	12.647	10.340	...
04189+2650(E)	FS Tau A	140(3)		04 22 02.18	+26 57 30.5	10.705	9.244	8.178	...
04189+2650(W)	FS Tau B, HH 157, Haro 6-5B	140(3)	0.6	04 22 00.70	+26 57 32.5	15.082	13.351	11.753	−0.04
04191+1523		140(7)	0.4	04 22 00.44	+15 30 21.2	16.592	12.354	11.259	0.97
04223+3700	L1478	350(1)	2.7	04 25 39.80	+37 07 08.2	...	13.170	10.271	0.47
04239+2436	HH 300 VLA 1 L1524	140(1)	1.1	04 26 56.30	+24 43 35.3	14.323	11.530	9.764	0.09
04240+2559	DG Tau	140(1)	3.5	04 27 04.70	+26 06 16.3	8.691	7.722	6.992	−0.26
04248+2612	L1521D, HH 31 IRS2, Barnard 217	140(1)	0.3	04 27 57.30	+26 19 18.4	11.619	10.270	9.741	0.52
04275+3452(N)		350(2)	1.2	04 30 47.79	+34 59 16.4	...	14.989	13.512	0.76
04275+3452(S)		350(2)		04 30 47.57	+34 58 24.3	...	15.151	13.440	...
04275+3531		350(1)	1.5	04 30 48.52	+35 37 53.2	...	...	15.268	0.51
04287+1801	L1551 IRS 5B, HH 154	140(1)	20.2	04 31 34.08	+18 08 04.9	12.230	10.550	9.255	0.76
04288+2417	HK Tau	140(1)	0.2	04 31 50.57	+24 24 18.1	10.451	9.253	8.593	0.30
04292+2422(E)	Haro 6-13	140(1)	0.6	04 32 15.41	+24 28 59.7	11.237	9.319	8.101	0.01
04292+2422(W)	L1529	140(1)		04 32 13.27	+24 29 10.8	13.364	9.906	8.124	...
04295+2251	L1536 IRS	140(1)	0.3	04 32 32.05	+22 57 26.7	14.889	11.982	10.141	0.13
04302+2247	HH 394, near L1536	140(1)	0.3	04 33 16.50	+22 53 20.2	13.489	11.772	10.876	1.34
04315+3617	L1483	350(2)	1.7	04 34 53.22	+36 23 29.2	12.503	10.838	9.616	−0.05
04325+2402	L1535 IRS, Barnard 18I	140(1)	0.7	04 35 35.39	+24 08 19.4	16.122	11.504	9.826	1.71
04327+5432	L1400, HH 378	170(1)	1.9	04 36 45.50	+54 39 04.5	16.437	13.974	12.618	0.84
04365+2535	TMC-1A, L1534	140(1)	1.9	04 39 35.19	+25 41 44.7	16.389	12.062	10.020	0.68
04368+2557	L1527 FIR, HH 192 VLA 1	140(1)	1.3	04 39 53.6[I]	+26 03 05.5	...	...	...	2.35
04369+2539	LBN 813, Barnard 14 L1527	140(1)	1.3	04 39 55.75	+25 45 02.0	10.668	8.052	6.275	−0.49
04381+2540	TMC-1, L1534	140(1)	0.6	04 41 12.68	+25 46 35.4	16.076	12.954	11.254	0.64

Table 1
(Continued)

IRAS	Associations	$D(pc)$[a]	$L_{\rm bol}$	α(J2000)[b]	δ(J2000)[b]	J[c]	H[c]	K_s[c]	α[d]
04530+5126	L1438, V347 Aur, RNO 33	none		04 56 57.02	+51 30 50.9	9.990	8.825	8.062	0.05
04591−0856	IC 2118	210(8)	0.9	05 01 29.64	−08 52 16.9	11.359	10.341	9.933	0.62
05155+0707	HH 114	460(17)	11.8	05 18 17.30	+07 10 59.9	…	12.567	10.214	1.55
05198+3325	cluster in NGC 1893	6000(24)	13481.	05 23 08.3[I]	+33 28 38	…	…	…	0.50
05256+3049		16500(4)	6417.3	05 28 49.86	+30 51 29.3	…	14.412	11.914	0.16
05283−0412	HH 58	460(25)	5.4	05 30 51.30	−04 10 32.2	…	…	13.628	1.00
05286+1203	S264	400(26)	14.4	05 31 27.79	+12 05 30.9	…	14.596	12.763	1.05
05289−0430		470(2)	7.1	05 31 27.09	−04 27 59.4	13.082	11.086	9.425	0.38
05302−0537	Haro 4-145	470(2)	42.7	05 32 41.65	−05 35 46.1	…	15.116	11.389	0.38
05311−0631	L1641, HH 83 VLA 1	470(3)	7.3	05 33 32.52	−06 29 44.2	13.358	11.487	9.749	0.23
05320−0300	RNO 45, S277	400(26)	5.4	05 34 31.09	−02 58 02.3	13.726	11.758	10.546	2.12
05327−0457(N)		450(9)		05 35 14.39	−04 55 22.6	…	…	…	…
05327−0457(E)		450(9)		05 35 19.32	−04 55 45.0	15.547	12.277	10.079	…
05327−0457(S)		450(9)		05 35 14.99	−04 56 04.5	…	…	13.316	…
05327−0457(W)	Ced 55e	450(9)	920.2	05 35 13.10	−04 55 52.5	13.166	10.886	9.360	1.76
05340−0603		470(2)	19.3	05 36 32.48	−06 01 16.4	17.243	14.253	12.268	1.47
05357−0650	L1641	480(1)	10.8	05 38 09.31	−06 49 16.6	9.938	8.969	7.978	0.01
05375−0040	Haro 5-90	470(2)	7.1	05 40 06.79	−00 38 38.1	10.913	9.496	8.514	0.62
05375−0731	L1641 S3 IRS	480(1)	70.0	05 39 53.51	−07 30 09.5	…	14.662	12.497	2.13
05378−0750(W)	L1641	480(1)	8.2	05 40 14.95	−07 48 48.5	…	15.392	13.470	0.25
05378−0750(E)		480(1)		05 40 17.81	−07 48 25.8	15.939	12.647	10.488	…
05379−0758	L1641	480(1)	6.4	05 40 20.55	−07 56 39.9	12.851	10.678	9.399	0.19
05384−0808	L1641 S4, S85	480(1)	10.8	05 40 50.59	−08 05 48.7	13.134	11.349	10.276	1.03
05391−0841	L1641	480(1)	3.6	05 41 30.05	−08 40 09.2	…	14.729	11.855	0.77
05399−0121	L1630, HH 92,	430(1)	10.7	05 42 27.7[I]	−01 20 02	…	…	…	1.53
05403−0818	L1641 S2	480(1)	9.9	05 42 47.07	−08 17 06.9	15.671	13.155	11.063	0.40
05404−0948	L1647	480(1)	49.8	05 42 47.67	−09 47 22.5	10.818	9.810	9.232	0.76
05405−0117	L1630	430(1)	4.4	05 43 03.06	−01 16 29.2	14.467	11.877	10.300	0.71
05413−0104	L1630, HH 212	430(1)	10.5	05 43 51.5[I]	−01 02 52	…	…	…	2.91
05417+0907	L1594, HH 175, Barnard 35A	465(1)	18.4	05 44 30.01	+09 08 57.1	…	15.913	12.400	1.68
05427−0116		470(2)	2.5	05 45 17.31	−01 15 27.6	14.666	12.195	10.740	0.63
05450+0019	L1630	430(1)	27.6	05 47 36.55	+00 20 06.3	11.406	9.604	8.784	1.26
05510−1018		470(2)	1.8	05 53 23.71	−10 17 27.6	16.267	15.085	12.787	0.93
05513−1024		470(2)	5.1	05 53 42.55	−10 24 00.7	9.803	7.635	5.956	0.18
05548−0935		470(2)	1.1	05 57 13.23	−09 35 10.9	14.573	13.357	12.544	0.72
05555−1405(N)	RNO 58	470(2)	4.8	05 57 49.46	−14 05 27.8	13.711	12.190	11.014	0.62
05555−1405(S)		470(2)		05 57 49.18	−14 06 08.0	13.480	12.138	11.085	…
05564−1329		470(2)	5.6	05 58 46.91	−13 29 18.8	14.021	12.061	10.762	0.38
05580−1034		470(2)	1.7	06 00 24.49	−10 34 49.5	…	15.520	14.058	0.53
05581−1026		470(2)	2.9	06 00 28.64	−10 26 31.9	17.464	…	14.701	0.47
05582−0950	RNO 60	470(2)	3.9	06 00 38.76	−09 50 38.5	…	13.255	11.783	1.26
05596−0903		470(2)	2.3	06 02 01.7[I]	−09 03 06	…	…	…	1.11
05598−0906(N)	GGD 10	470(2)	14.3	06 02 16.20	−09 06 29.0	14.553	11.876	9.813	0.43
05598−0906(S)		470(2)		06 02 15.52	−09 06 53.0	13.182	11.314	10.337	…
06010−0943	NGC 2149	425(20)	48.7	06 03 28.1[I]	−09 43 57	…	…	…	1.50
06027−0714		830(1)	8.7	06 05 07.90	−07 14 42.6	16.226	13.473	12.607	1.08
06033−0710		830(1)	10.3	06 05 48.61	−07 10 31.2	…	…	…	1.28
06047−1117		500(10)	4.9	06 07 08.50	−11 17 51.0	14.119	12.222	10.220	0.64
06053−0622	Mon R2	830(19)	29143.	06 07 46.7[I]	−06 23 00	…	…	…	0.74
06057−0923		830(2)	7.0	06 08 05.29	−09 23 47.3	…	…	…	0.97
06216−1044		830(2)	7.1	06 24 01.78	−10 45 53.5	…	14.365	11.614	0.14
06249−0953	L1652	830(1)	6.4	06 27 17.34	−09 55 27.4	15.034	13.652	12.559	1.04
06297+1021(E)		900(2)	46.8	06 32 30.83	+10 18 39.6	13.640	11.095	9.244	0.32
06297+1021(W)		900(2)		06 32 26.12	+10 19 18.4	10.884	9.316	8.025	…
06368+0938	L1613	790(11)	6.5	06 39 32.09	+09 35 41.5	…	…	…	0.93
06381+1039		960(4)	143.6	06 40 58.15	+10 36 52.1	…	…	14.513	1.93
06382+0939	NGC 2264 IRS 2 cluster	910(18)	512.6	06 41 02.7[I]	+09 36 10	…	…	…	1.13
06382+1017	L1610/1613 HH 124	800(3)	84.4	06 41 02.64	+10 15 02.1	13.362	12.218	10.592	1.00
06393+0913		950(4)	28.9	06 42 08.13	+09 10 30.0	15.243	12.048	10.593	1.42
07018−1005(E)		1150(2)	30.3	07 04 13.93	−10 10 13.6	14.764	12.560	10.866	0.35
07018−1005(W)		1150(2)		07 04 09.86	−10 10 18.7	15.800	13.135	11.868	…

Table 1
(Continued)

IRAS	Associations	$D(pc)$[a]	L_{bol}	α(J2000)[b]	δ(J2000)[b]	J[c]	H[c]	K_s[c]	α[d]
07025−1204(N)		1150(27)		07 04 50.71	−12 09 14.8	13.622	11.985	10.708	...
07025−1204(S)		1150(27)	49.5	07 04 51.62	−12 09 29.9	...	13.865	11.832	1.29
07028−1100		1150(2)	190.0	07 05 12.69	−11 04 29.9	16.847	14.155	12.242	0.96
07161−2336		1500(29)	30.2	07 18 15.65	−23 41 32.8	...	15.189	14.079	1.86
07178−4429		450(28)	18.1	07 19 28.26	−44 35 11.5	8.579	7.285	6.080	−0.28
07180−2356	L1660, HH 72 IRS	1500(17)	186.0	07 20 08.36	−24 02 23.0	...	14.176	11.648	0.81
07334−2320		1770(4)	30.2	07 35 34.51	−23 26 49.6	...	...	14.787	0.75
07339−2403	L1666	1790(4)	42.1	07 36 04.79	−24 10 17.1	...	...	14.066	0.68
07499−3306		1830(4)	42.9	07 51 50.8[l]	−33 14 43	...	...	...	0.97
07576−3718		1370(4)	30.9	07 59 28.6[l]	−37 26 33	...	...	...	1.44
08043−3343(N)		1120(4)	14.6	08 06 15.61	−33 52 19.5	...	15.274	13.016	0.39
08043−3343(S)		1120(4)		08 06 15.32	−33 52 35.3	...	15.937	13.985	...
08128−4357		none		08 14 33.97	−44 07 05.3	13.016	11.453	10.439	0.01
08261−5100		450(30)	4.8	08 27 39.00	−51 10 39.3	12.562	10.520	9.043	0.09
08373−4059		1340(4)	107.9	08 39 12.0[l]	−41 10 05	...	...	...	0.99
08375−4109		700(12)	284.0	08 39 19.93	−41 19 50.5	...	12.980	9.470	0.68
08393−4041		1350(48)	361.4	08 41 06.76	−40 52 17.4	9.273	8.236	7.471	1.40
09049−4650		700(50)	13.6	09 06 39.0[l]	−47 02 12	...	...	...	2.04
09099−4526	VdBH 29a	700(50)	13.7	09 11 46.86	−45 38 56.1	12.206	10.385	9.609	0.95
09116−4522		700(50)	9.0	09 13 27.44	−45 34 33.3	16.132	13.440	11.931	0.64
09204−4752		700(50)	169.0	09 22 12.49	−48 05 03.8	10.998	8.730	7.147	0.60
09212−4556		700(50)	6.7	09 23 02.1[l]	−46 09 13	...	...	...	−0.08
09343−4522		700(50)	3.0	09 36 14.08	−45 36 04.5	...	...	...	0.64
11072−7727	Ced 111 IRS 5, HH 909 Chamaeleon IR Nebula	140(31)	14.3	11 08 38.20	−77 43 51.1	11.535	11.788	8.404	0.44
11101−5829	HH 136	2700(32)	11540.	11 12 18.19	−58 46 20.8	12.212	9.966	8.646	1.08
11590−6452		200(33)	9.0	12 01 36.40	−65 08 55.7	15.251	14.030	11.315	1.48
12277−6319		175(34)	6.6	12 30 34.5[l]	−63 36 23	...	...	...	1.08
12512−6122		none		12 54 18.1[l]	−61 38 19	...	...	...	0.83
12571−7654		200(35)	0.3	13 00 55.3[l]	−77 10 40	...	...	...	0.23
13030−7707		200(35)	0.2	13 06 57.45	−77 23 41.5	10.841	9.579	8.755	−0.15
13036−7644		200(35)	1.0	13 07 36.1[l]	−77 00 05	...	...	...	1.20
13050−6154		2000(36)	1174.0	13 08 12.25	−62 10 25.0	...	...	12.018	1.43
13054−6159		4000(51)	104106.	13 08 35.39	−62 15 06.9	15.393	13.183	11.875	1.32
13224−5928		1000(37)	45.6	13 25 41.36	−59 43 47.3	12.846	10.874	9.399	0.57
13294−6011		none		13 32 42.67	−60 26 54.2	...	12.861	10.763	1.21
13547−3944		550(38)	79.1	13 57 43.95	−39 58 47.1	8.865	8.069	7.264	0.62
14159−6111		1170(26)	4073.1	14 19 42.86	−61 25 12.1	...	14.080	11.583	1.78
14451−6502	VdBH 63	450(34)	6.0	14 49 17.6[l]	−65 15 22	...	...	...	0.32
14563−6301		450(34)	10.2	15 00 22.71	−63 13 25.3	10.993	9.354	8.216	0.36
14564−6254	HH 77	450(34)	28.2	15 00 37.15	−63 06 52.2	16.455	13.184	10.887	1.03
14568−6304	HH 139	1000(3)	85.6	15 00 58.58	−63 16 55.0	11.733	10.064	8.763	−0.31
15107−5800		none		15 14 41.20	−58 11 49.9	15.909	12.319	8.507	1.83
15115−6231		1260(39)	66.5	15 15 41.08	−62 42 38.1	13.079	11.141	10.293	1.38
15215−6056		170(??)	0.5	15 25 39.6[l]	−61 06 51	...	...	...	1.50
15398−3359	HH 185, Lupus 1, Barnard 228	170(3)	1.4	15 43 01.32	−34 09 15.3	15.963	13.992	12.326	1.59
15420−3408	HT Lup	159(49)	1.2	15 45 12.86	−34 17 30.6	7.573	6.866	6.480	0.00
15420−4553		none		15 45 37.02	−46 02 30.9	13.834	11.613	10.097	0.28
16235−2416	ρ Oph S1	160(1)	159.7	16 26 34.17	−24 23 28.3	8.859	7.261	6.317	1.34
16240−2430(E)	L1681	160(1)	25.6	16 27 09.43	−24 37 18.8	16.788	11.049	7.140	0.24
16240−2430(W)		160(1)		16 27 02.34	−24 37 27.2	14.164	10.478	8.064	...
16288−2450(E)	L1689 IRS 5, ρ Oph S	160(1)	5.5	16 32 02.22	−24 56 16.8	...	13.813	10.726	0.70
16288−2450(W)	ρ Oph S	160(1)		16 31 52.98	−24 56 24.6	11.783	9.391	7.557	...
16289−4449	HH 57 IRS, V346 Nor	150(34)	5.9	16 32 32.19	−44 55 30.7	10.178	8.599	7.176	−0.04
16293−2422	ρ Oph East	160(1)	23.7	16 32 22.8[l]	−24 28 33	...	...	...	3.69
16295−4452		150(34)	1.9	16 33 07.73	−44 58 24.7	...	15.086	12.270	0.79
16316−1540	L43, RNO 91	160(1)	11.4	16 34 29.29	−15 47 01.9	10.994	9.635	8.464	0.84
16442−0930	L260	160(1)	0.7	16 46 58.27	−09 35 19.7	14.316	12.339	10.721	0.22
16544−1604		160(40)	1.1	16 57 20.12	−16 09 36.6	...	...	13.921	1.98
17364−1946	L219	none		17 39 23.25	−19 47 54.7	...	...	13.757	0.96
17369−1945	L219	none		17 39 55.95	−19 46 35.6	...	14.994	12.305	0.37
17441−0433	L425	none		17 46 50.89	−04 34 33.7	16.700	15.270	13.325	0.50
18148−0440	L483 FIR	225(1)	11.1	18 17 29.8[l]	−04 39 38	16.188	12.640	10.790	1.36

Table 1
(Continued)

IRAS	Associations	$D(pc)$[a]	L_{bol}	α(J2000)[b]	δ(J2000)[b]	J[c]	H[c]	K_s[c]	α[d]
18250−0351	NZ Ser	280(41)	219.7	18 27 39.53	−03 49 52.0	6.127	4.387	3.041	0.20
18264−0143		none		18 29 05.31	−01 41 56.9	...	...	13.968	1.39
18270−0153(E)		none		18 29 38.92	−01 51 06.3	...	15.321	12.874	...
18270−0153(W)		none		18 29 36.69	−01 50 59.1	13.700	11.797	10.711	0.49
18273+0034		none	1.4	18 29 53.06	+00 36 06.4	16.256	13.349	11.855	1.15
18274−0212		none		18 30 01.36	−02 10 25.6	...	15.145	11.489	0.12
18275+0040		700(42)	3.4	18 30 06.17	+00 42 33.6	9.833	8.605	7.516	−0.19
18278−0212		none		18 30 27.28	−02 11 00.2	...	...	14.550	1.62
18318−0434		none		18 34 31.73	−04 31 30.9	15.141	12.170	10.709	1.04
18331−0035	L588, HH 109, HH 108 IRAS	310(3)	3.8	18 35 42.00	−00 33 22.1	16.347	13.911	11.738	2.02
18339−0224		2200(43)	313.5	18 36 34.33	−02 21 49.0	...	14.505	13.304	1.32
18340−0116		none		18 36 38.54	−01 13 35.4	...	...	13.028	1.10
18341−0113	L564	none		18 36 46.33	−01 10 29.5	14.849	11.974	10.229	0.91
18358−0112		none		18 38 25.41	−01 10 10.2	...	13.770	12.089	1.24
18383+0059		none		18 40 51.87	+01 02 12.9	14.892	11.748	9.602	0.50
18527+0203		none		18 55 14.82	+02 07 47.8	14.253	11.078	9.556	1.67
18558+0041		none		18 58 23.01	+00 45 34.2	16.968	13.338	11.346	1.24
18561+0032		none		18 58 40.9[l]	+00 36 49	...	...	...	1.46
18577−3701	S CrA	130(44)	1.5	19 01 08.61	−36 57 20.1	8.194	7.051	6.107	−0.18
18583−3657	TY CrA	130(44)	21.6	19 01 40.82	−36 52 33.7	7.486	6.970	6.673	0.62
18585−3701	R CrA	130(44)	44.3	19 01 53.68	−36 57 08.2	6.935	4.951	2.858	0.12
18595−3712	ISO-CrA 182	129(13)	1.2	19 02 58.70	−37 07 34.1	...	15.881	14.498	1.83
19247+2238		none		19 26 51.33	+22 45 13.4	11.095	9.881	9.175	0.50
19266+0932	Parsamian 21 HH 221	300(3)	3.4	19 29 00.86	+09 38 42.9	11.205	10.485	9.763	0.37
19411+2306		2100(14)	3026.1	19 43 17.94	+23 14 01.6	13.946	11.548	9.596	1.11
20353+6742	L1152, HH 376	370(1)	1.4	20 35 46.33	+67 53 02.0	15.263	14.230	13.254	1.41
20355+6343	L1100	450(6)	2.5	20 36 22.86	+63 53 40.4	13.885	11.797	10.339	0.59
20361+5733	L1041	none		20 37 20.8[l]	+57 44 13	...	...	...	1.91
20377+5658	L1036	440(1)	4.8	20 38 57.48	+57 09 37.6	13.925	11.226	9.507	0.32
20386+6751	L1157 IRS, HH 375 VLA 1	370(1)	5.5	20 39 06.6[l]	+68 02 13	...	...	...	2.23
20436+5849		910(4)	24.0	20 44 49.3[l]	+59 00 18	...	...	...	1.31
20453+6746	PV Cep, HH 215, L1158	500(3)	63.7	20 45 53.94	+67 57 38.7	12.453	9.497	7.291	−0.32
20568+5217	L1002, HH 381 IRS	1270(4)	45.6	20 58 21.09	+52 29 27.7	11.544	9.813	8.305	0.62
20582+7724	L1228, HH 199	175(1)	1.2	20 57 12.94	+77 35 43.7	13.024	10.608	9.171	0.31
21004+7811	HH 198, RNO 129	300(3)	13.5	20 59 14.03	+78 23 04.1	9.437	7.530	6.319	0.20
21007+4951	L988	700(1)	31.1	21 02 23.85	+50 03 06.8	16.368	14.818	13.276	0.69
21017+6742(E)	L1172	288(15)		21 02 29.94	+67 54 08.3	15.022	12.035	10.415	...
21017+6742(W)	L1172	288(15)	0.5	21 02 21.27	+67 54 20.1	...	...	14.890	0.66
21023+5002	cluster	1420(4)	873.0	21 03 57.6[l]	+50 14 38	...	...	...	0.00
21025+5221		none		21 04 07.45	+52 33 53.5	...	...	12.896	1.12
21025+6801	L1172B	288(2)	2.6	21 03 14.24	+68 12 14.2	14.710	12.669	11.789	1.14
21169+6804	L1177, CB 230	450(6)	7.3	21 17 38.69	+68 17 33.4	11.562	9.898	9.188	1.75
21352+4307	Barnard 158	600(6)	11.7	21 37 11.39	+43 20 38.4	...	15.877	12.915	0.17
21388+5622	HH 588	750(16)	96.5	21 40 28.98	+56 35 55.7	12.801	11.620	10.789	0.59
21391+5802	L1121, IC 1396N	750(16)	254.2	21 40 42.80	+58 16 01.1	...	15.642	14.155	2.15
21418+6552	cluster	1380(4)	3432.8	21 43 02.3[l]	+66 06 29	...	...	...	1.15
21432+4719	HH 379 IRS	900(45)	26.1	21 45 08.23	+47 33 05.6	14.643	13.169	11.914	1.07
21445+5712	IC 1396 East	360(4)	18.5	21 46 07.12	+57 26 31.8	13.950	11.965	10.139	0.54
21454+4718	L1031B, V1735 Cyg	900(1)	106.7	21 47 20.66	+47 32 03.6	9.889	8.087	7.040	0.70
21461+4722		900(2)	7.0	21 48 00.4[l]	+47 36 38	...	...	...	1.07
21569+5842	L1143	250(4)	1.0	21 58 35.90	+58 57 22.8	15.457	12.936	10.695	0.08
22051+5848	L1165, HH 354 IRS	750(3)	73.0	22 06 50.37	+59 02 45.9	11.370	10.248	9.682	1.15
22176+6303	L1240, RAFGL 2884, S 140 IRS1-3	910(1)	21313.	22 19 20.39	+63 19 38.5	12.304	9.298	6.135	0.87
22266+6845	L1221, HH 363	200(1)	1.8	22 28 02.99	+69 01 16.7	16.575	13.544	11.465	0.53
22267+6244	L1203	900(1)	311.2	22 28 29.4[l]	+62 59 44	15.826	11.799	9.244	1.45
22272+6358(E)	L1206	950(1)	815.5	22 28 57.60	+64 13 37.5	13.728	10.530	8.250	1.76
22272+6358(W)		950(1)		22 28 50.83	+64 13 44.8	...	14.944	12.483	...
F22324+4024	V375 Lac, LkHα 233	880(3)	111.6	22 34 41.01	+40 40 04.5	11.294	10.307	8.921	0.08
22376+7455	L1251B 3, HH 189	330(1)	10.7	22 38 47.02	+75 11 34.7	...	...	13.194	1.09
22451+6154	L1211	1290(4)	822.5	22 47 02.12	+62 10 05.4	14.941	12.401	10.855	1.20

Table 1
(Continued)

IRAS	Associations	$D(pc)$[a]	$L_{\rm bol}$	α(J2000)[b]	δ(J2000)[b]	J[c]	H[c]	K_s[c]	α[d]
22457+5751	cluster	4460(4)	25778.	22 47 46.5^I	+58 07 19	...	...	...	1.19
22517+6215		1030(4)	58.8	22 53 40.5^I	+62 31 59	...	...	...	1.45
23037+6213(E)	Cep C	1190(4)	330.2	23 05 49.76	+62 30 01.2	12.510	10.408	9.045	1.23
23037+6213(W)		1190(4)		23 05 45.77	+62 30 21.5	15.853	14.988	12.923	...
23238+7401	L1262 SMM 1	200(1)	0.9	23 25 46.6^I	+74 17 38	...	...	...	1.23
F23591+4748		none		00 01 43.25	+48 05 19.0	13.322	11.592	10.404	0.60

Notes.
RNO designates objects in "Red and Nebulous Objects in Dark Clouds: a Survey" (Cohen 1980).
[a] The estimated distance to each source in parsecs. The citation for the distance estimate is designated by the number in the parenthesis, and are as follows: (1) Hilton & Lahulla 1995; (2) Educated guess based on proximity to nearby objects; (3) Reipurth 1999; (4) Wouterloot & Brand 1989; (5) Obayashi et al. 1998; (6) Launhardt & Henning 1997; (7) André et al. 1999; (8) Kun et al. 2001; (9) Mookerjea et al. 2000; (10) Yun et al. 2001; (11) Sagar & Joshi 1983; (12) Moreira et al. 2000; (13) Marraco & Rydgren 1981; (14) Guetter 1992; (15) Straizys et al. 1992; (16) Battinelli & Capuzzo-Dolcetta 1991; (17) Reipurth & Aspin 1997; (18) Neri et al. 1993; (19) Racine 1968; (20) Wilson et al. 2005; (21) Guetter & Turner 1997; (22) Heyer et al. 1996; (23) Karr & Martin 2003; (24) Marco et al. 2001; (25) Reipurth et al. 1993; (26) Sugitani et al. 1991; (27) Sugitani & Ogura 1995; (28) Sugitani & Ogura 1994; (29) Launhardt & Henning 1997; (30) Vilas-Boas et al. 2000; (31) Cambresy et al. 1998; (32) Tamura et al. 1997; (33) Bourke 2001; (34) Gregorio-Hetem et al. 1988; (35) Hughes & Hartigan 1992; (36) Sugitani & Ogura 1994; (37) Henning & Launhardt 1998; (38) Maheswar et al. 2004; (39) Mikami & Ogura 1994; (40) Huard et al. 1999; (41) Bachiller et al. 2001; (42) Zhang et al. 1988; (43) Birkmann et al. 2006; (44) Knude & Hog 1998; (45) Davis et al. 2001; (46) Hachisuka et al. 2006; (47) Aspin & Sandell 1997; (48) Wouterloot & Brand 1999; (49) Prato et al. 2003; (50) Liseau et al. 1992; (51) Clark & Porter 2004; none = Searched for and could not find a distance estimate
[b] 2MASS coordinate for candidate YSO. When a near-IR counterpart could not be identified in the 2MASS images, a superscript "I" designates an *IRAS* coordinate.
[c] Magnitudes from the 2MASS extended source catalog, in the 2MASS photometric system.
[d] α is the spectral index of the source (Lada 1991).
(This table is also available in a machine-readable form in the online journal)

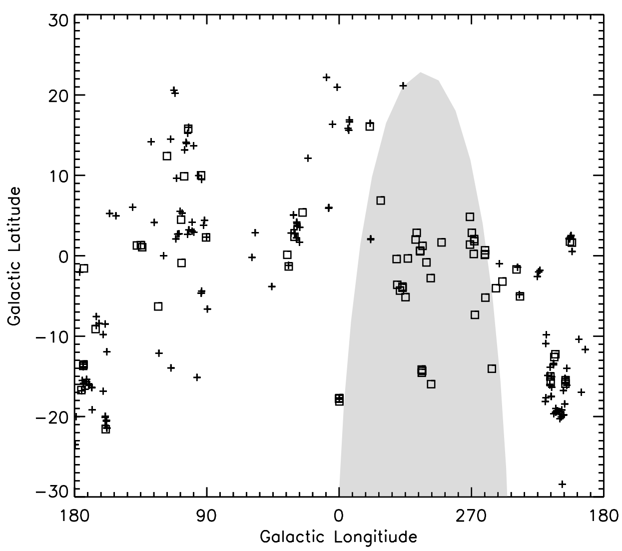

Figure 3. Location of our Class I sources in Galactic coordinates. The crosses are the targets we observed and the squares are targets that we did not observe, usually because they are too far south, there is no embedded near-IR counterpart to the *IRAS* source, or the source is an embedded cluster. The shaded area to the right is south of $\delta = -40°$, and never rises above two airmasses from Mauna Kea. All of our targets are within 30° of the Galactic plane.

while others are Class 0 objects, or a filament or knot in a cloud. A few of the stars in our sample are examples of what have become known as "transitional" objects, i.e. objects between Class I and T Tauri stars with a spectral index near 0. These sources were observed as they satisfied our selection criteria and since the studies by Haisch et al. (2004) and Duchêne et al. (2004) include such objects. We did not attempt to observe the Class 0 objects since there is typically no flux in the near-IR. In some cases, *MSX* (Price et al. 2001) observations showed that an *IRAS* point source was a knot or a filament in a cloud, and not a true point source. Such sources have no near-IR counterpart and were not observed.

3.2. Observation Methods

Previous studies of the Class I binary frequency (Haisch et al. 2004; Duchêne et al. 2004) searched for binary companions at the K band. We found that the seeing was better and more stable at L' than at the K band, and that reflection nebulae (which tend to have blue colors) are much less of a problem at L'. The bright sky background at L' also made it more difficult to see stars without an IR excess, reducing the effect of background star contamination. We therefore focused our search for binary companions on our L' observations, and used the K-band and H-band observations for additional photometry.

Since we wanted to observe a large number of targets from H through L', we chose telescope/instrument combinations that have this capability in one instrument, have good image quality, and have a suitable plate scale. We used the UH 2.2 m telescope with QUIRC (1024^2 HgCdTe 1–2.5 μm 3′ field of view (FOV), Hodapp et al. 1996), the NASA IRTF with the SpeX guider (512^2 InSb 1–5 μm 1′ FOV, Rayner et al. 2003) and NSFCam2 (2048^2 Hawaii-2RG 1–5.5 μm 82″ FOV), UKIRT with UIST (1024^2 InSb 1–5 μm 1′ FOV, Ramsay Howat et al. 2004), and Subaru Telescope with CIAO (1024^2 InSb 1–5 μm 22″ FOV, Murakawa et al. 2004) and IRCS (1024^2 InSb 1-5 μm 1′ FOV, Tokunaga et al. 1998 and Kobayashi et al. 2000). Table 2 lists which telescopes were used on which nights. The majority of our observations used UKIRT and UIST, primarily due to the availability of observing time. Due to UKIRT's north declination limit of +60°, IRTF observations targeted sources north of this limit up to the north declination limit of IRTF (+70°). We used Subaru to observe targets north of this, targets for which we did

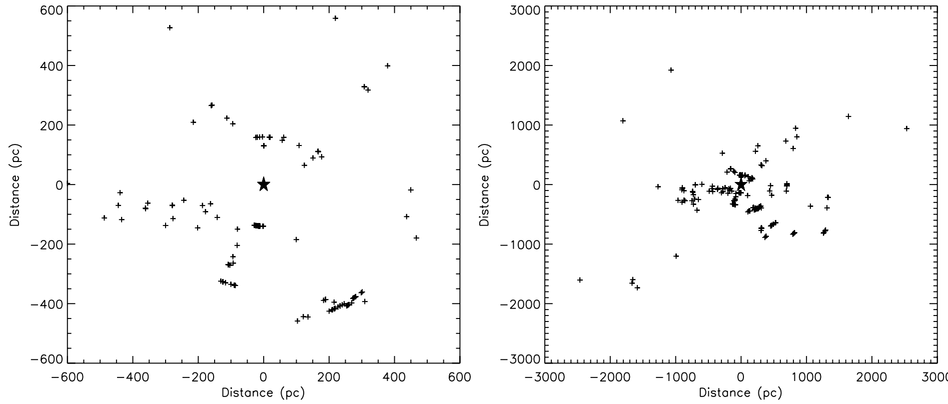

Figure 4. Location of our Class I sources looking down on the Galactic plane. The left panel shows sources out to a radius of 600 pc while the right panel shows sources out to a radius of 3 kpc. The Sun is represented by the star symbol in the center of the figure. The Galactic center is toward the top, the Taurus star-forming region is just below the Sun, and the Orion star-forming region is to the lower right.

Table 2
Observing Nights

Date (UT)	Observatory	Instr.	Weather
2003 Nov 2–5	UKIRT	UIST	4 nights photometric
2003 Nov 29–30	UKIRT	UIST	1.5 nights lost
2004 Feb 11–15	UKIRT	UFTI	4 photometric half-nights
2004 May 15–17	UKIRT	UIST	3 half-nights lost
2004 May 24–25	UKIRT	UIST	2 half-nights, 0.25 night lost
2004 May 26–29	IRTF	SpeX	36 hours, photometric
2004 Jun 19–21	UKIRT	UIST	0.5 night lost
2004 Jul 29	UH 2.2 m	QUIRC	1 night, photometric
2004 Aug 2	Subaru	IRCS	0.5 nights lost, poor seeing
2004 Aug 3–5	UH 2.2 m	QUIRC	3 nights, 1.75 nights lost
2004 Nov 5	IRTF	SpeX	0.5 nights, clear
2004 Nov 18	IRTF	SpeX	0.5 nights, clear
2004 Dec 4–9	IRTF	SpeX	5 half-nights, 1.5 nights lost, poor seeing
2004 Dec 30–31	UKIRT	UIST	1.5 nights, 1 night lost
2005 Nov 16–18	Subaru	CIAO	3 nights, 1 non-photometric

not get good image quality with IRTF, and to observe targets with adaptive optics (AO).

Dithering was used for all observations in order to remove bad pixels and the detector flat field effects. A 3×3 dither pattern was typically used, the size of which was usually $5''$–$10''$and depended on the field of view of the instrument and the availability of guide stars. In the case of L' observations, coadds were used to increase the effective integration time per dither position to ∼20 s to increase observing efficiency. Standard stars that have been observed by UKIRT through the MKO filter set (Simons & Tokunaga 2002; Tokunaga & Simons 2002) were selected from the UKIRT faint standard star list, and were observed for photometric calibration. Furthermore, the instruments we used have MKO filters, and thus all of our observations are in the MKO photometric system.

All data were reduced using the following procedure except in the case of the IRTF data, where the data were first divided by the product of the number of coadds and the number of non-destructive reads. A dark frame was made by averaging together ten individual darks of the same exposure time as the science data. This dark frame was then subtracted from each target frame. To make the sky frame, each dark subtracted frame was scaled to have the same median value, then averaged together using a min–max rejection. The resulting sky frame was then normalized using the median value of the pixel counts. Each dark subtracted (non-scaled) target frame was divided by this normalized sky flat. The median sky value for each frame was subtracted from each frame to set the average background counts in each frame to 0. The images were then aligned and averaged together using an average sigma clipping rejection. In addition, images with better than average resolution were combined into a higher resolution image. This rejects images where the seeing was particularly poor or where there was a guiding error. Since most of the L' "sky" brightness is from the telescope, the procedure we used was not optimal for making a true L' flat field. However, the L' flats we used were effective for removing the detector's flat-field response.

For this project, having the best angular resolution possible was critical. Particular attention was paid on maintaining the best focus possible. In the case of our IRTF observations with the SpeX guider, the image resolution was often limited by aberrations either in the telescope or in the instrument. Aberrations in UIST on UKIRT also occasionally limited our resolution at K, but rarely at L'. We used the $0\farcs06$ plate scale in UIST in order to be able to use a longer exposure time at L' and to better sample the point-spread function (PSF). The resulting $1'$ FOV also allowed objects within 4500 AU of the target to be in the field of view for the closest targets. The angular resolution distributions at H, K, and L' are presented in Figure 5. The median FWHM was $0\farcs609$ at the H band, $0\farcs543$ at the K band, and $0\farcs335$ at the L' band. The L'-band median FWHM includes our AO observations.

Table 3
AO Observed Sample

IRAS	r (″)[a]	B[b]	R[b]	I[b]	Date
04240+2559	1.4	10.13	8.97	7.65	2005 Nov 14
04530+5126	0.5	17.80	13.69	11.35	2005 Nov 14
05289−0430E	0.4	17.51	14.96	14.54	2005 Nov 15
05289−0430W	17.1	17.51	14.96	14.54	2005 Nov 15
05302−0537	27.5	16.83	14.42	13.13	2005 Nov 14
05327−0457W	35.7	17.71	15.89	14.18	2005 Nov 15
05357−0650	0.3	12.98	10.52	10.38	2005 Nov 15
05375−0040	5.5	16.37	14.04	12.63	2005 Nov 14
05384−0807	37.1	9.94	8.03	7.82	2005 Nov 15
05404−0948	0.6	18.41	15.16	12.96	2005 Nov 15
05513−1024	3.0	12.91	11.79	9.47	2005 Nov 15
05555−1405N	6.1		11.26	9.62	2005 Nov 15
05555−1405S	17.0		10.52	9.69	2005 Nov 15
06297+1021W	0.5	19.29	15.95	14.11	2005 Nov 15
06382+1017	17.3	17.38	14.09	14.53	2005 Nov 14
07025−1204N	15.5	17.86	15.10	13.06	2005 Nov 15
07025−1204S	5.2	17.86	15.10	13.06	2005 Nov 15
08043−3343	33.1	14.37	13.11	12.54	2005 Nov 15
19247+2238	10.7	17.24	14.35	12.72	2005 Nov 14
20453+6746	1.8	16.86	15.72	11.10	2005 Nov 14
20568+5217	0.3	19.90	13.74	12.13	2005 Nov 15
21388+5622	15.4	17.61	13.97		2005 Nov 15
21454+4718	1.9	20.70	16.11	12.95	2005 Nov 15
22376+7455	0.1	16.18	14.65	13.55	2005 Nov 15

Notes.
[a] The separation from the guide star to the target.
[b] The USNO magnitudes of the guide star.

3.3. AO Observations

The selection of targets in nearby dark clouds naturally selected against nearby bright stars that could be used as AO guide stars. To find sources with a suitable visual guide star, we searched through the USNO-B1.0 catalog (Monet et al. 2003) for stars within 40″of the near-IR source that are brighter than R or $I = 16$. The objects that we observed with AO are presented in Table 3. To reduce the chance of reflection nebulosity interfering with our search for very close companions, we only observed sources with no resolved nebulosity in our seeing-limited L'-band data.

There are a number of cases where enough of the visible light from the YSO is able to escape the cloud to use the YSO itself as a guide star. This raises the possibility that the AO observed sub-sample is, on average, older and more evolved than the sample as a whole. We used the Kolmogorov–Smirnov test to determine if the AO observed sub-sample is different from the whole sample based on the spectral index and bolometric luminosity distributions. The whole sample and the AO observed sub-sample are not statistically different with regard to spectral index or bolometric luminosity at the 3σ level.

3.4. Target Fields

Figure 6 shows a $20'' \times 20''$(3000 AU to 10^5 AU, depending on distance) field around each target at L'. For targets where multiple near-IR sources do not fit within this field, more than one field is shown. Each near-IR source is labeled with a number that corresponds to that object's photometry presented in Table 4 if there is more than one object in the field. The inset images show regions of interest in more detail. In some cases, the primary star has been subtracted to better show a companion star in the inset image.

3.5. Photometry

We obtained H-, K-, and L'-band data in order to use the near-IR colors to separate embedded YSOs from foreground or background stars. We used archival Canada–France–Hawaii Telescope (CFHT) Skyprobe data to ensure that the data we used for photometry were taken under photometric conditions, characterized by a stable attenuation measurement near 0 throughout the night. On nights that were non-photometric, the photometry was calibrated using field stars in our photometric data or in 2MASS. If we used 2MASS for H- and K-band photometry and we have our own L' observations, the variability of our targets affects the accuracy of the colors that we derive, since the target may have varied in brightness between the 2MASS observations or between the 2MASS and our observations. We also converted the 2MASS photometry to the MKO system. Aperture photometry was performed using IMEXAMINE in IRAF using five aperture sizes (typically 0$''$.9, 1$''$.2, 1$''$.5, 1$''$.8, 2$''$.1) while maintaining the same buffer and sky annulus width (both typically 1$''$.8) for each aperture size. The same procedure was used for our standard stars. We compared the brightness of the target and the standard using the same aperture size to derive a magnitude estimate for each of the five aperture sizes. We then averaged these five estimates together, taking the standard deviation of these measurements as the accuracy to which we could measure the photometry of that individual source given the quality of the data. We made an airmass correction plot using our standard star data. We used the standard deviation of the standard star photometry from the best-fit linear airmass extinction curve as the lower limit to our photometric errors. This error was combined with the individual measurement error via a Pythagorean sum (root of summed squares) to estimate the total photometric error for each object in each filter (δH, δK, and $\delta L'$ in Table 4). We used the airmass extinction values in Krisciunas (1987) for our airmass correction.

4. BINARY DETECTION

All binary stars were found by visual inspection of our images. We found that Fourier filtering of our PSF-subtracted images (described below) did not enhance the visibility of close or faint companions since the PSF-subtraction residuals had the same spatial size as a real companion. We did not attempt to use an automated star finding program on account of our previous experience with programs such as DAOFIND. As an example, if the search parameters were set to find faint stars, then it would also identify positions without a star. Since our fields only had a few objects, a star-finding program was not necessary.

4.1. Contrast Limit

Visual surveys for binary stars are always sensitive to contamination from background stars. One way to minimize background star contamination is by adopting a contrast limit, such that any star fainter than the limit is not considered as a potential companion since the possibility of such a faint star being background contamination is unacceptably high and the chance of it being a real companion is acceptably low. Haisch et al. (2004) used a contrast limit of $\Delta K = 4$, whereas Reipurth & Zinnecker (1993) adopted a $\Delta z = 5$ contrast limit. Duquennoy & Mayor (1991) found that nearly all main-sequence binary stars with a solar-type primary have a mass ratio greater than 10:1. In light of this, we should choose an L'-band contrast limit that allows for all binaries with a mass ratio greater than 10:1. Reipurth

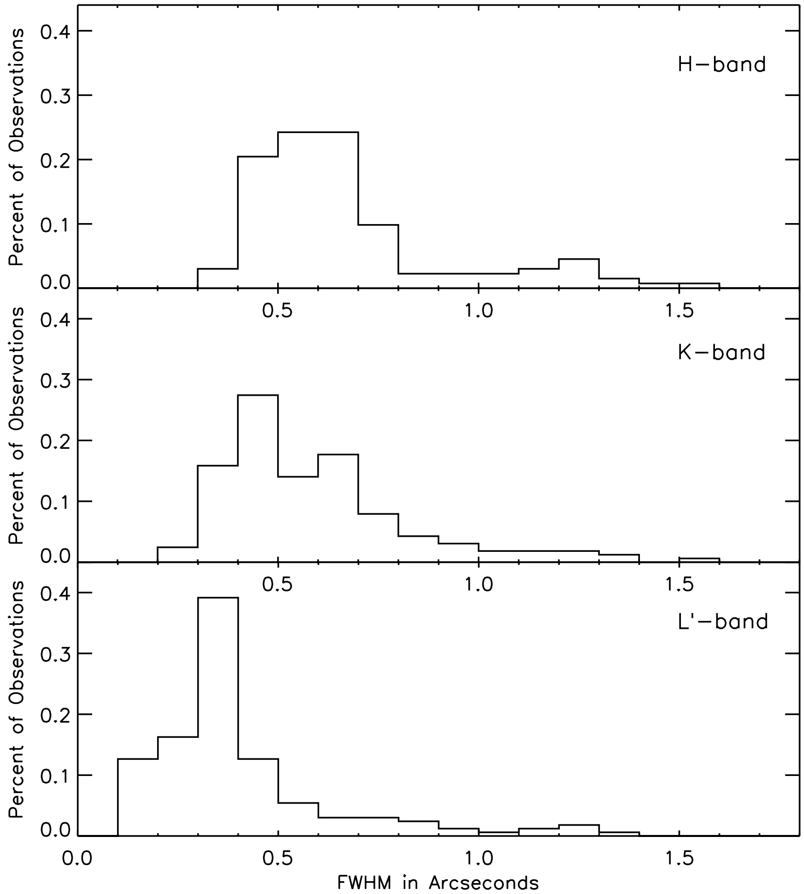

Figure 5. Angular resolution distributions at H, K, and L'. The median angular resolution (FWHM) is 0$''$.609 at H, 0$''$.543 at K, and 0$''$.335 at L'.

Table 4
Target Photometry

IRAS	#[a]	H	δH[b]	Date	K	δK[b]	Date	L'	$\delta L'$[b]	Date
00182+6223	1	14.71	0.14	2004 Jul 28	13.16	0.08	2004 Jul 28	11.36	0.05	2004 Aug 01
00182+6223	2	18.11	0.04	2004 Jul 28	15.39	0.05	2004 Jul 28	13.37	0.14	2004 Aug 01
00182+6223	3	15.11	0.05	2004 Jul 28	14.15	0.05	2004 Jul 28	13.01	0.08	2004 Aug 01
00465+5028		14.94	0.18	2003 Nov 03	12.65	0.08	2003 Nov 04	9.96	0.05	2003 Nov 02
		...	...	...	...	...	...	9.79	0.04	2004 Jun 19
01166+6635		13.60	0.06	2004 Jul 28	12.30	0.06	2004 Jul 28	10.69	0.04	2004 Aug 01
02086+7600		11.90	0.04	2004 Jul 28	10.99	0.05	2004 Jul 28	...	...	...
02310+6133		...	...	...	...	...	...	...	...	...
02511+6023		...	...	...	...	...	...	...	...	...
03220+3035	1	12.16	0.04	2003 Nov 04	10.83	0.05	2003 Nov 01	8.43	0.05	2003 Nov 03

Notes.
Photometry includes flux from this source and an adjacent source, which were not resolved in this wavelength.
[a] The identifier of the L' source in the finder chart.
[b] The photometric uncertainty in this filter, as described in Section 3.5.
(This table is available in its entirety in a machine-readable form in the online journal. A portion is shown here for guidance regarding its form and content)

& Zinnecker (1993) state that for coeval stars on the Hayashi track, the flux ratio approaches the mass ratio as the wavelength increases, with these ratios being effectively equal at 2.2 μm. Consider a binary system with a mass ratio (and thus a photospheric flux ratio) of 10:1, where only the primary star has an infrared excess. In this case, the primary star's infrared excess can be up to three times greater than its photospheric flux without the observed flux ratio of the binary exceeding 40:1. Thus, a contrast limit of $\Delta L' = 4$ satisfies our criteria for not excluding a significant number of real companions.

4.2. Artificial Binary Detection and the Inner Detection Limit

The angular resolution of the images, the contrast between the primary star and the companion, and, to a lesser degree, the plate scale of the camera affected how close we were able to detect

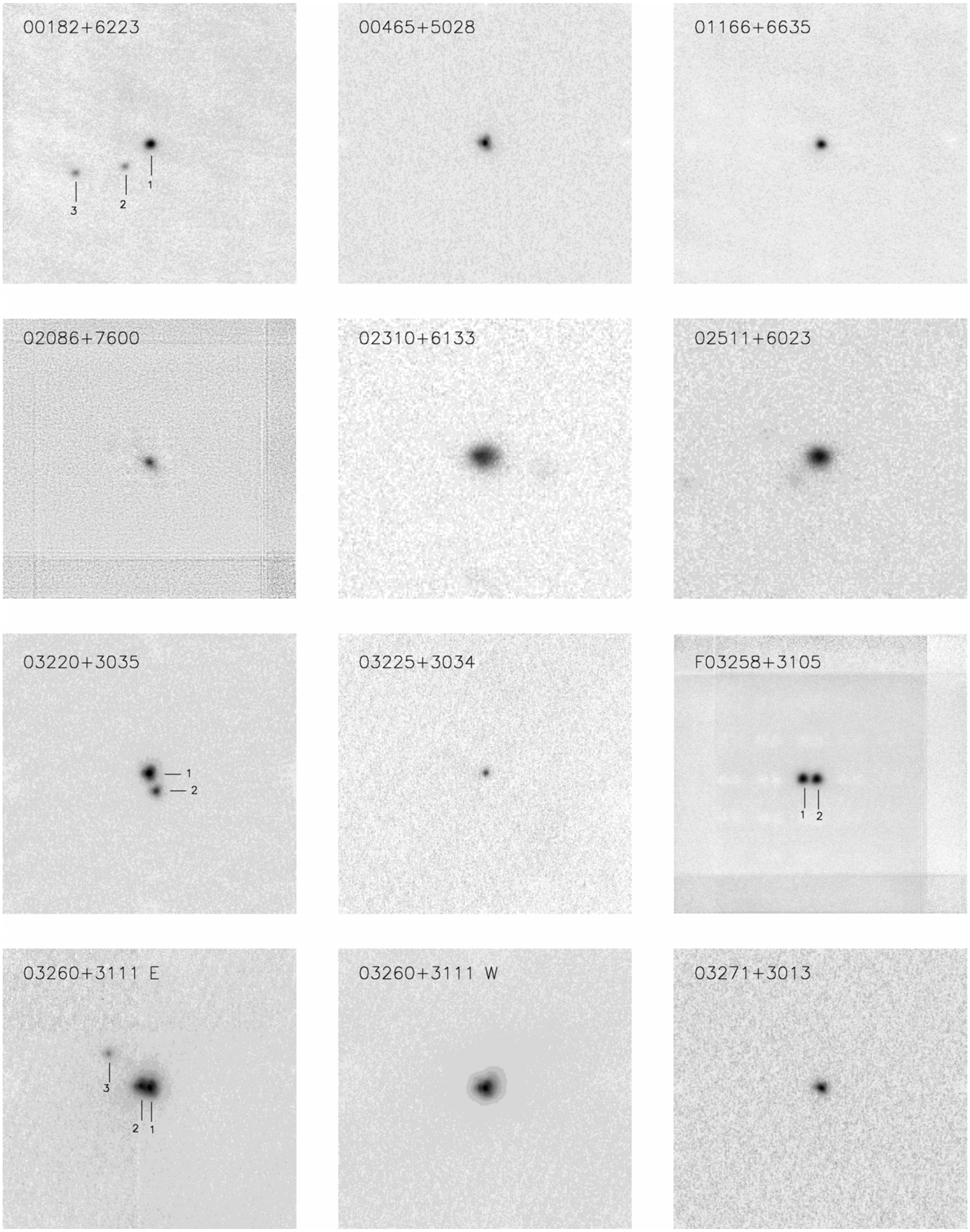

Figure 6. Images of each of our targets at L'. A $20'' \times 20''$field is shown.

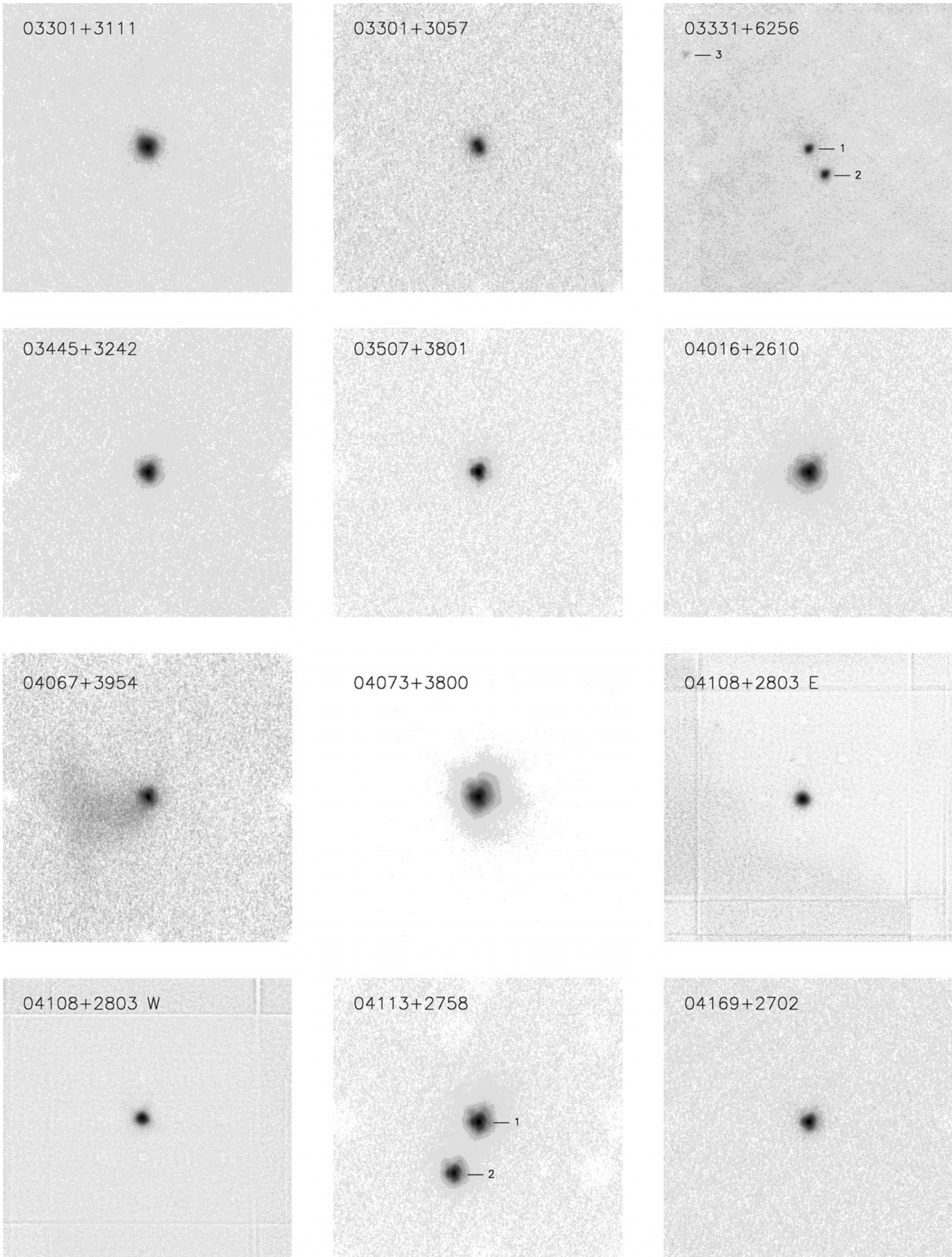

Figure 6. (Continued)

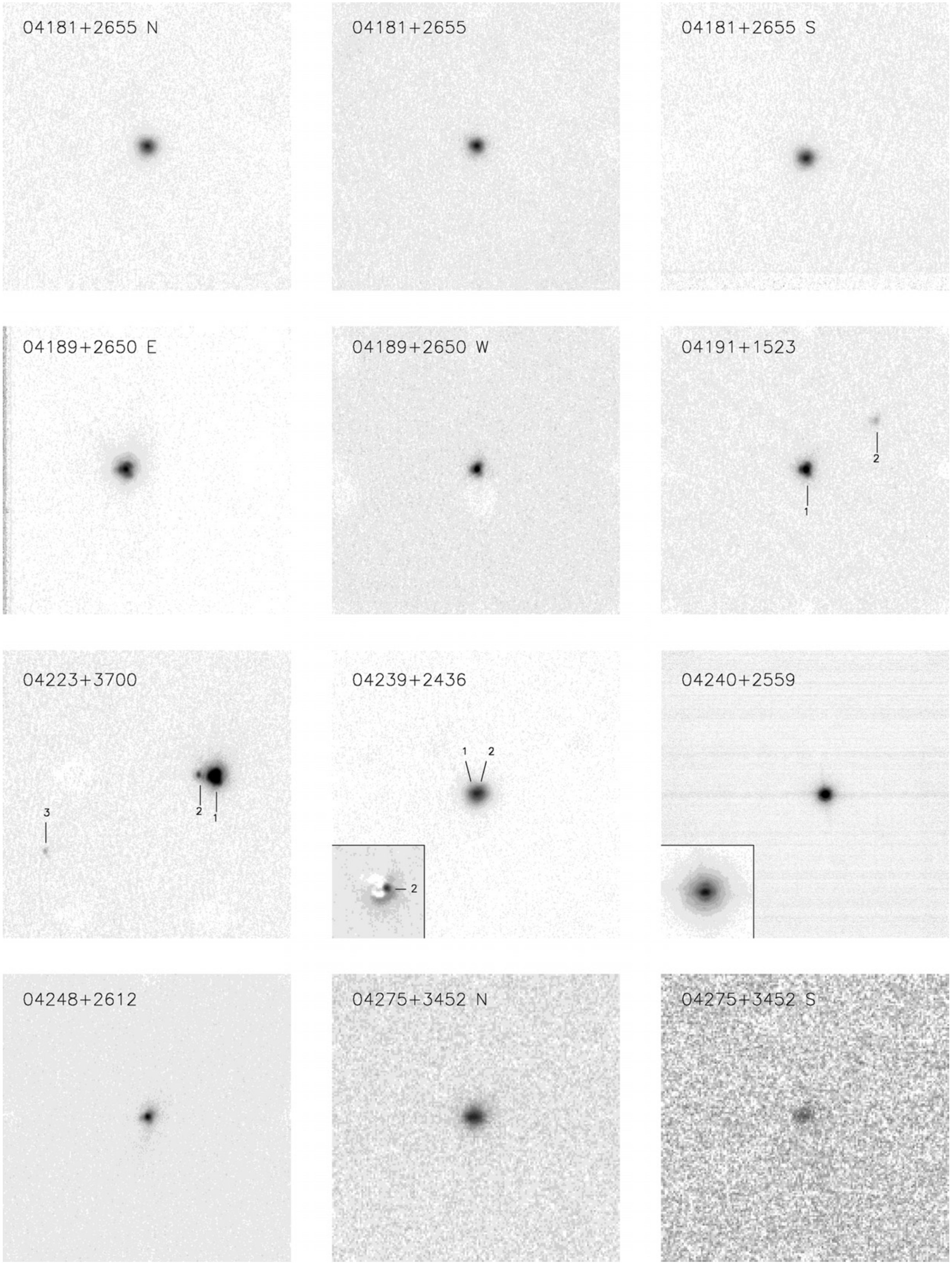

Figure 6. (Continued)

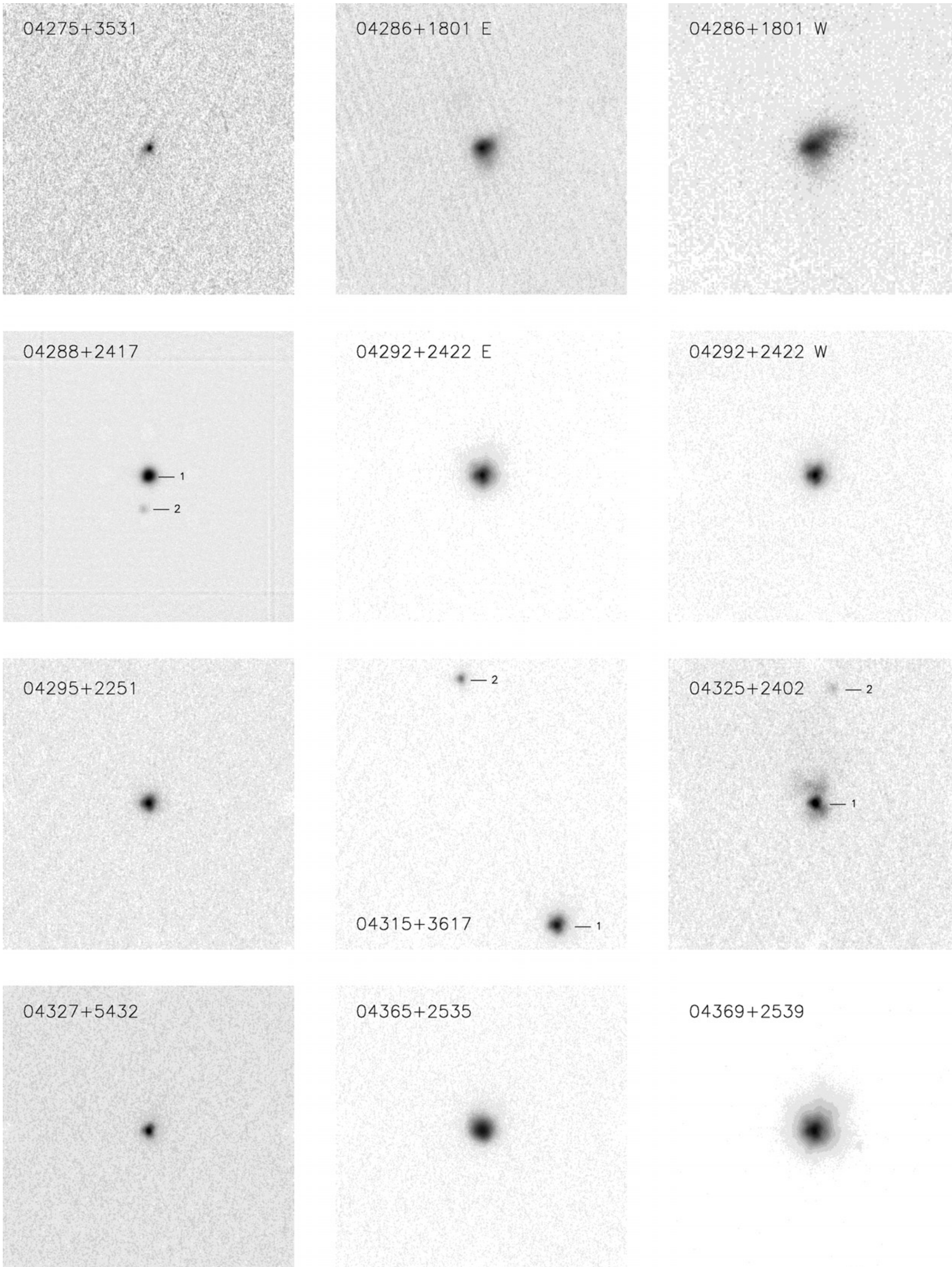

Figure 6. (Continued)

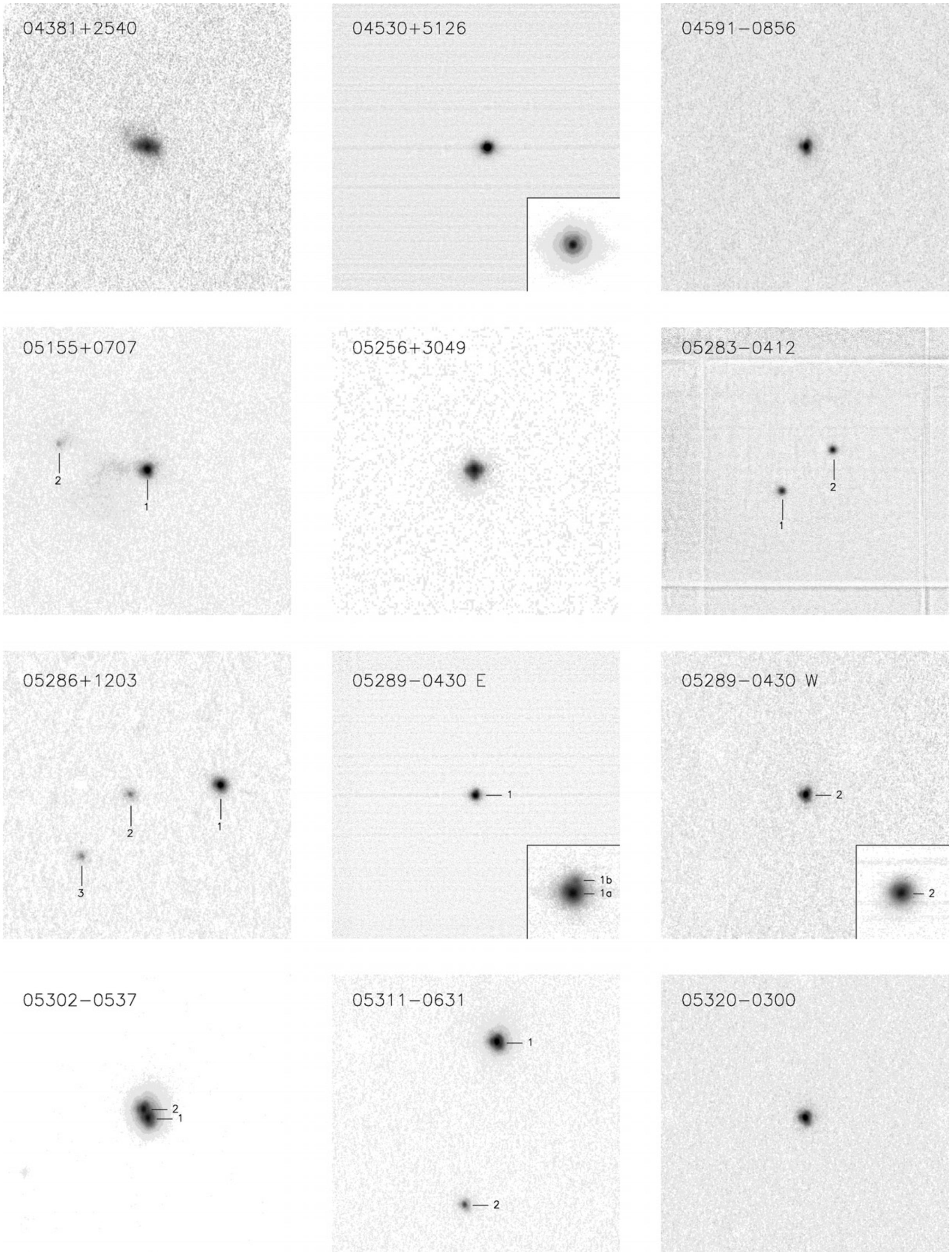

Figure 6. (Continued)

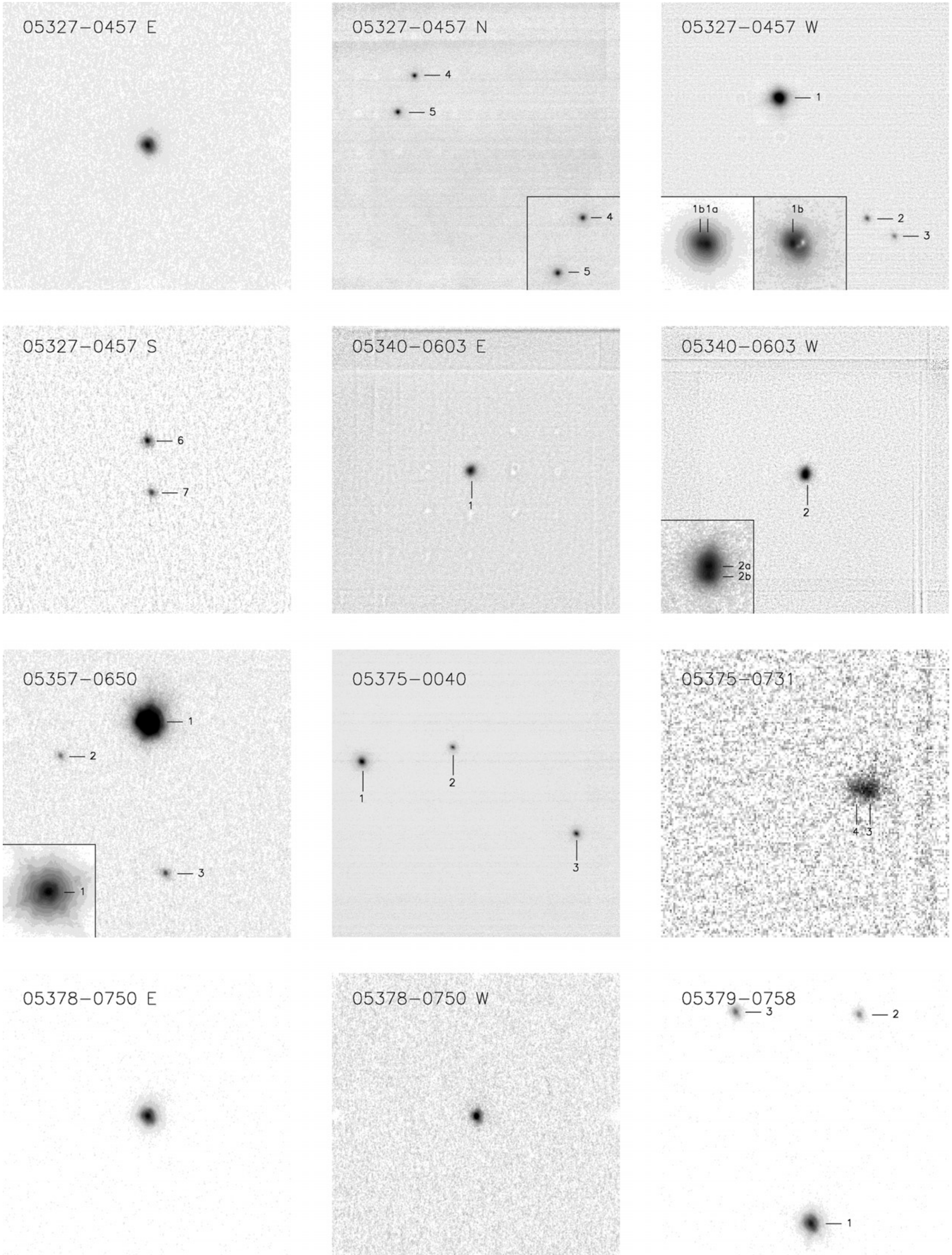

Figure 6. (Continued)

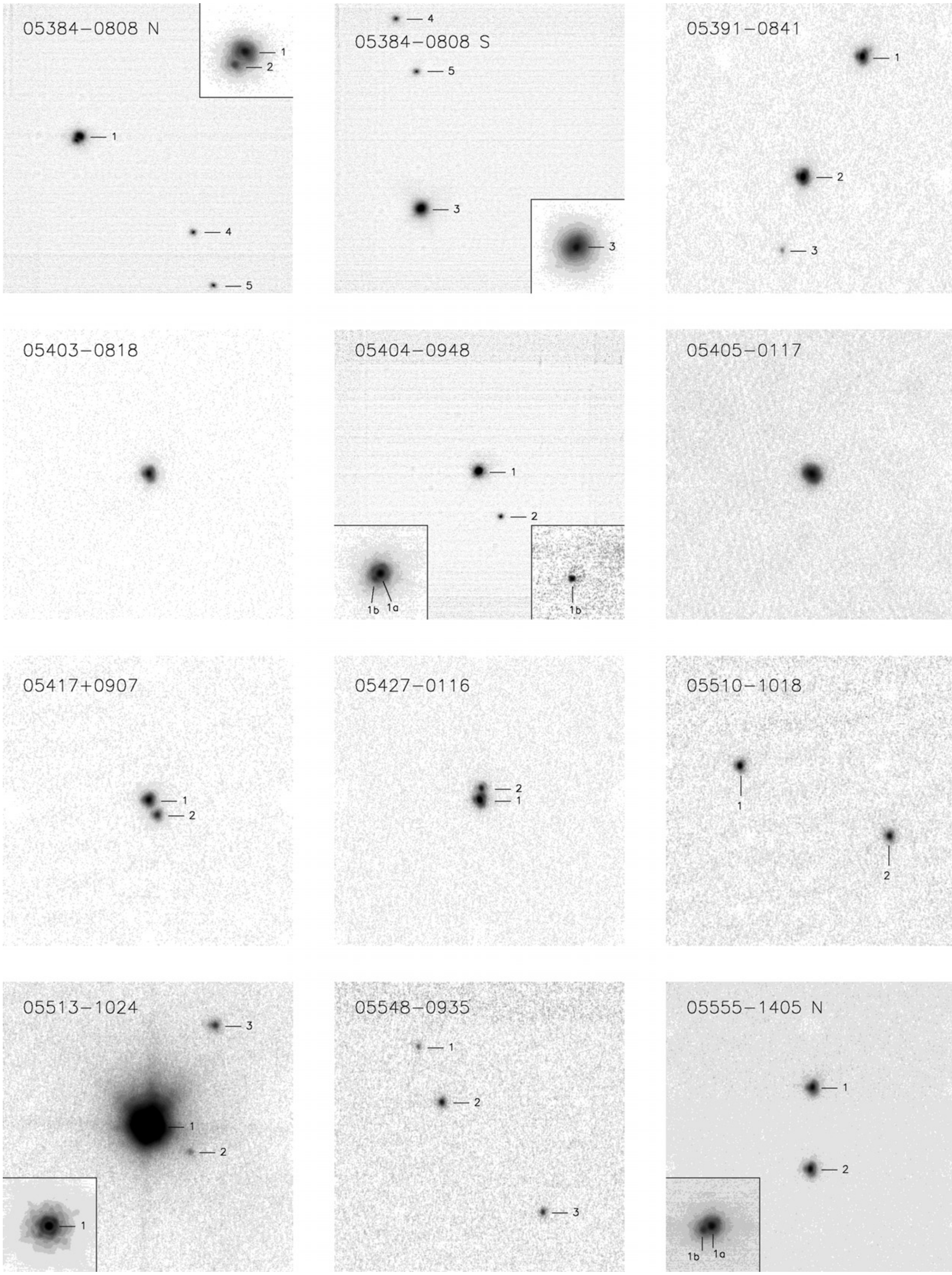

Figure 6. (Continued)

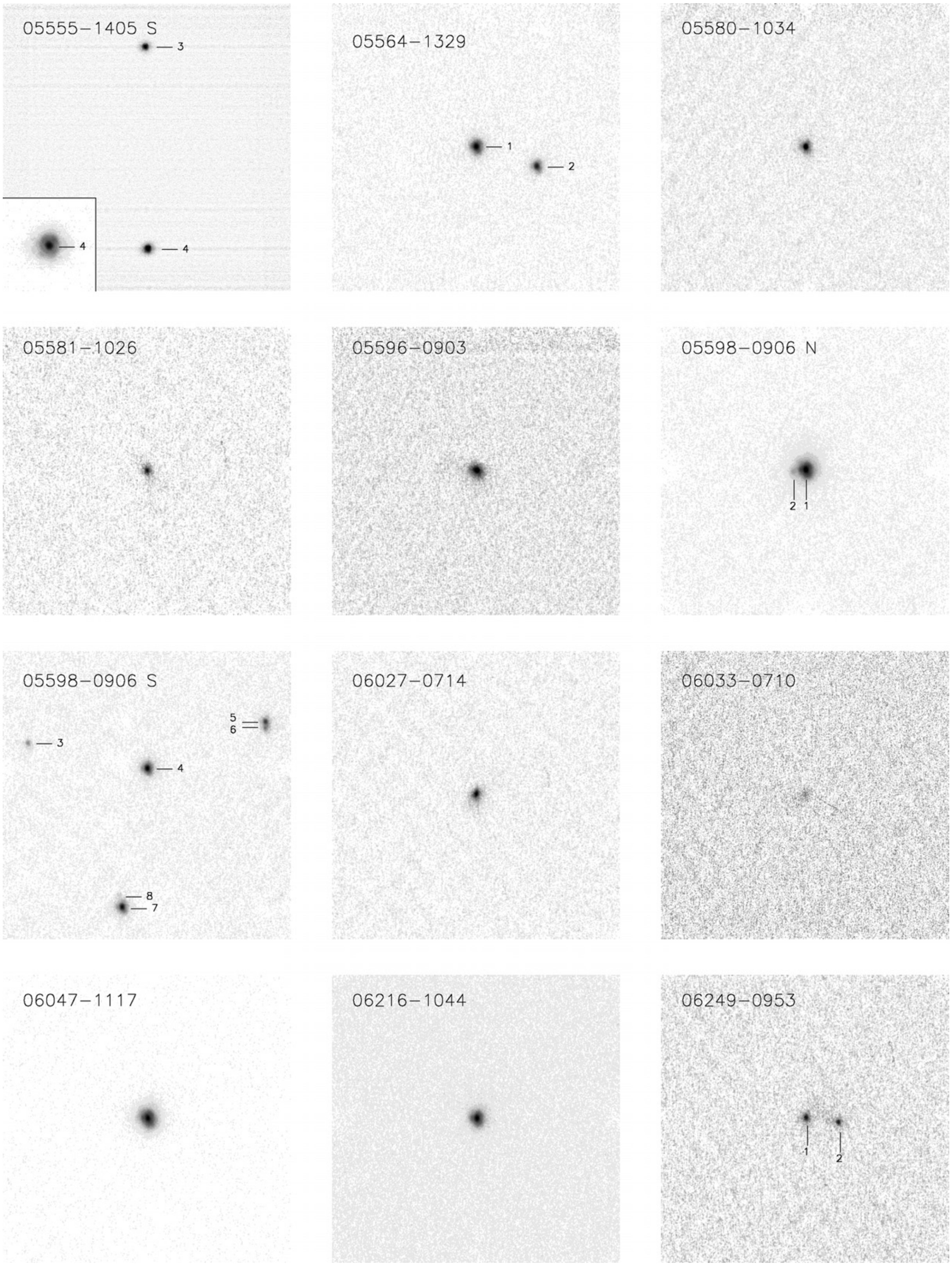

Figure 6. (Continued)

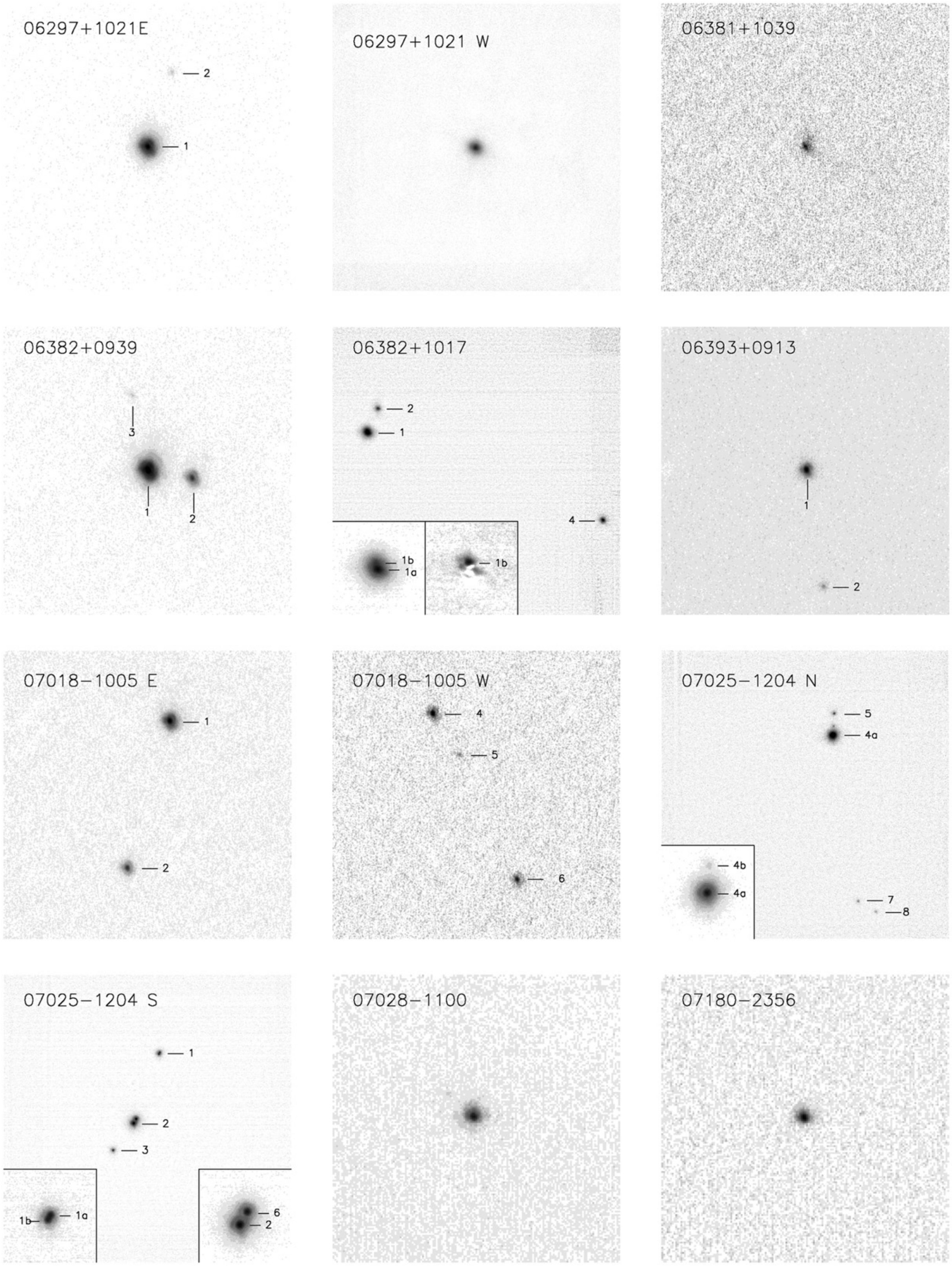

Figure 6. (Continued)

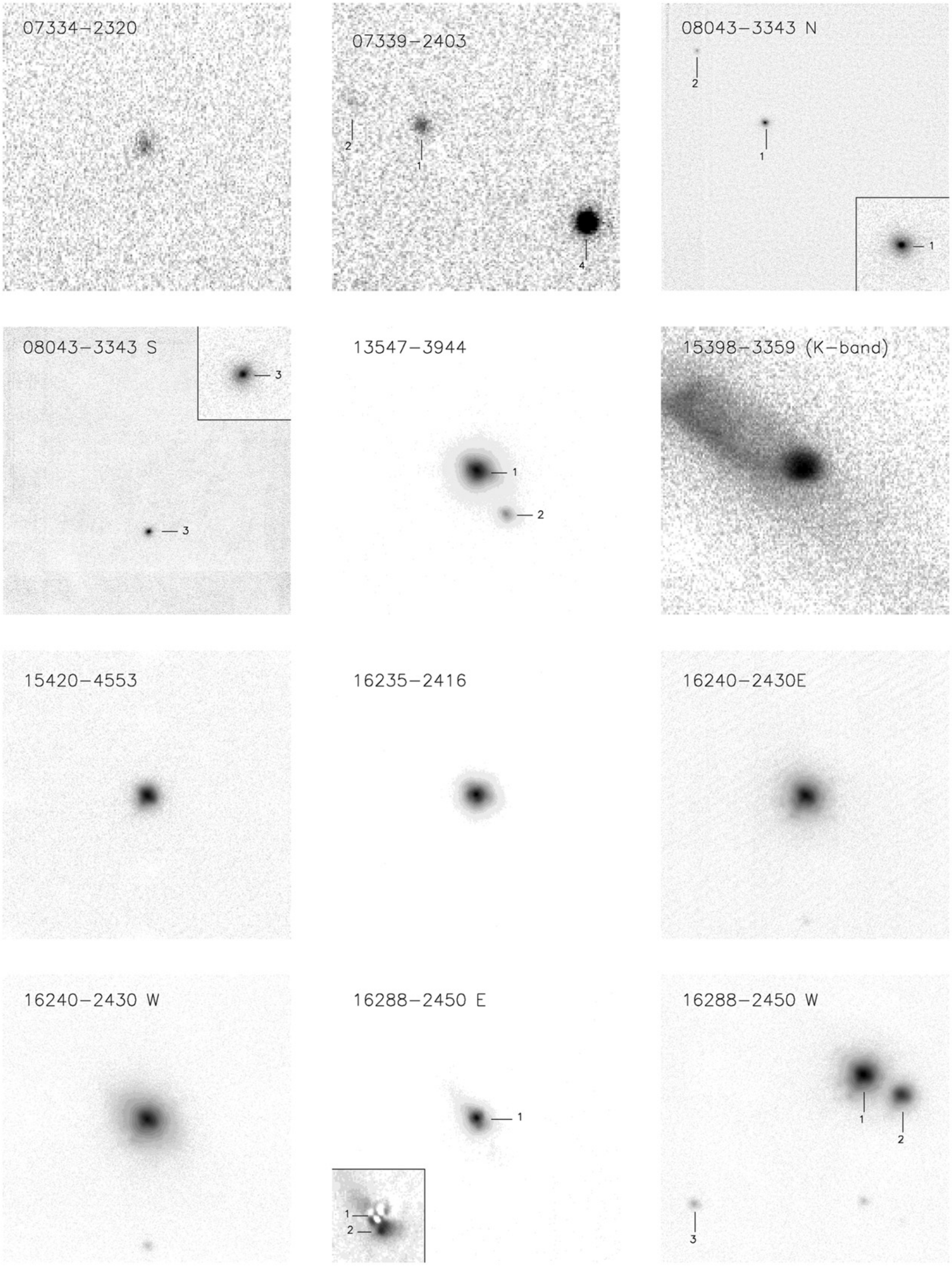

Figure 6. (Continued)

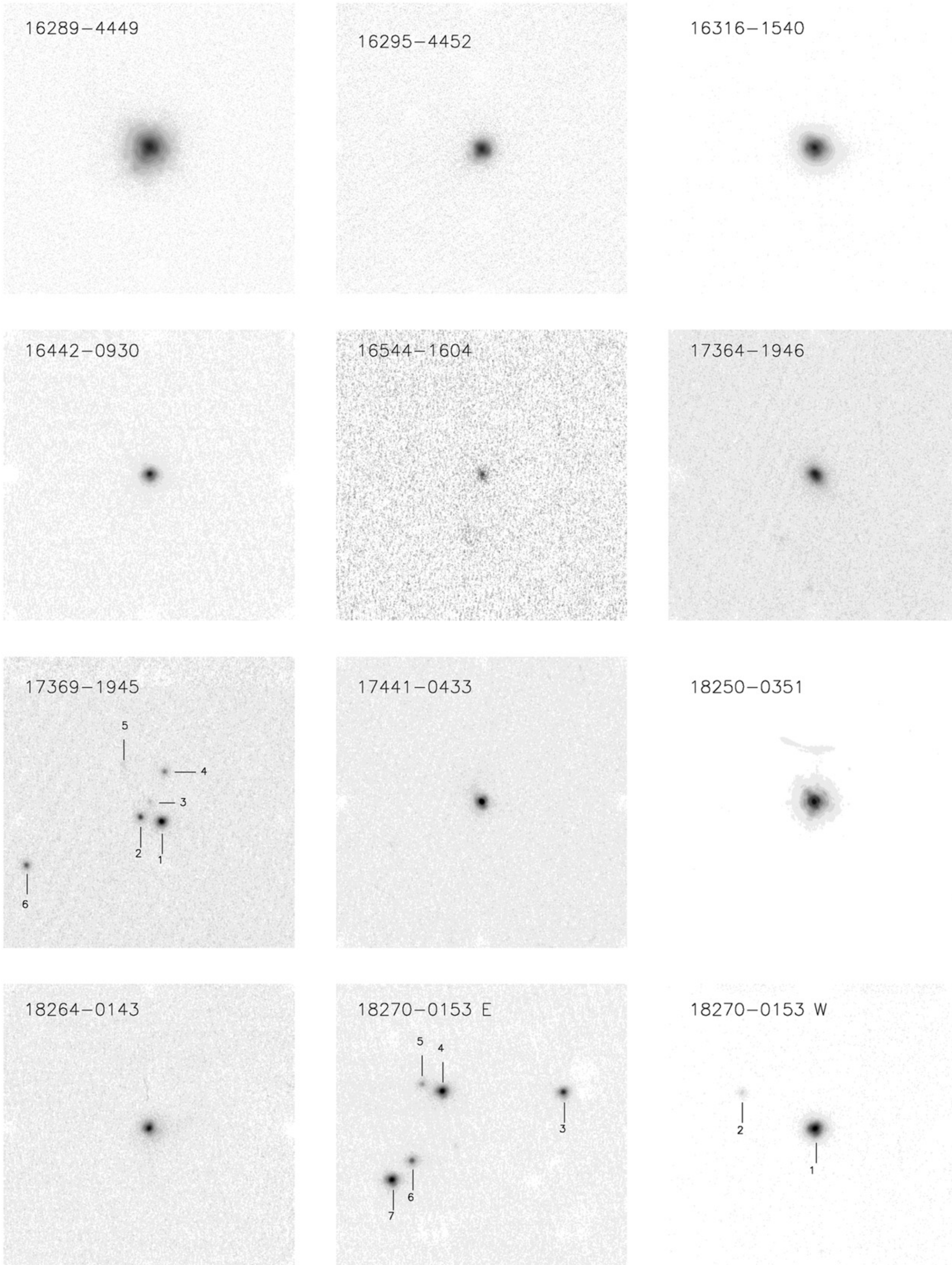

Figure 6. (Continued)

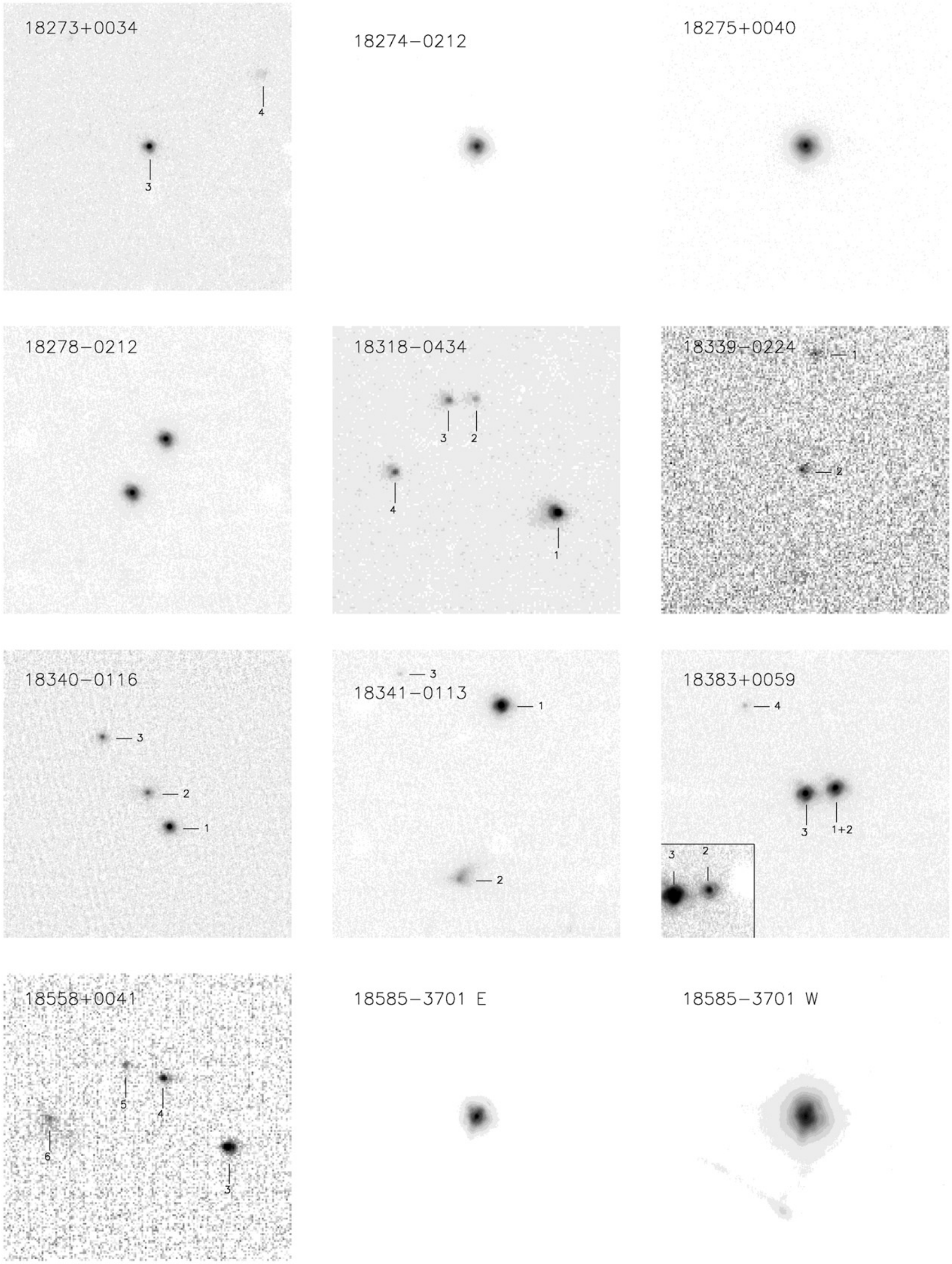

Figure 6. (Continued)

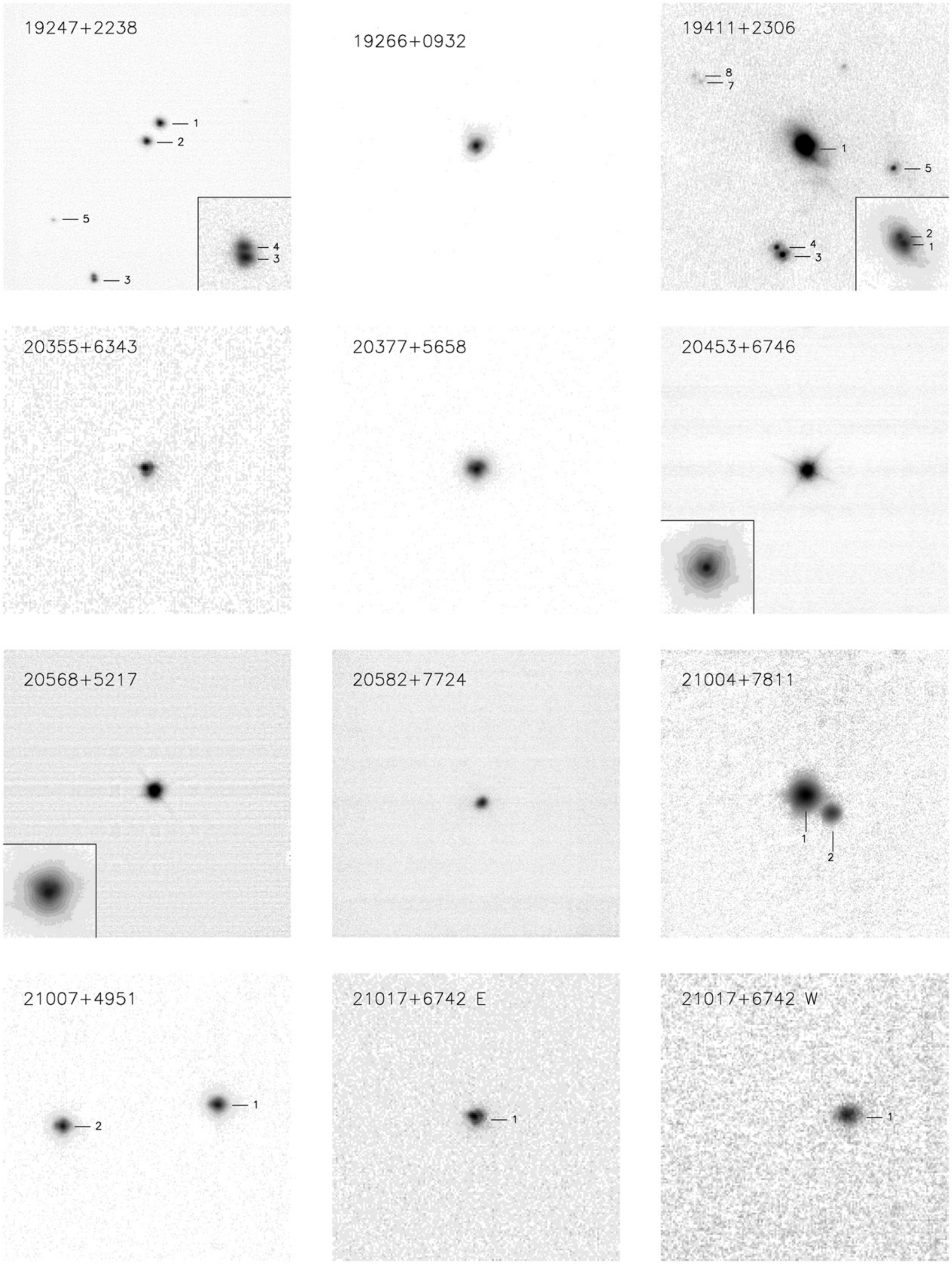

Figure 6. (Continued)

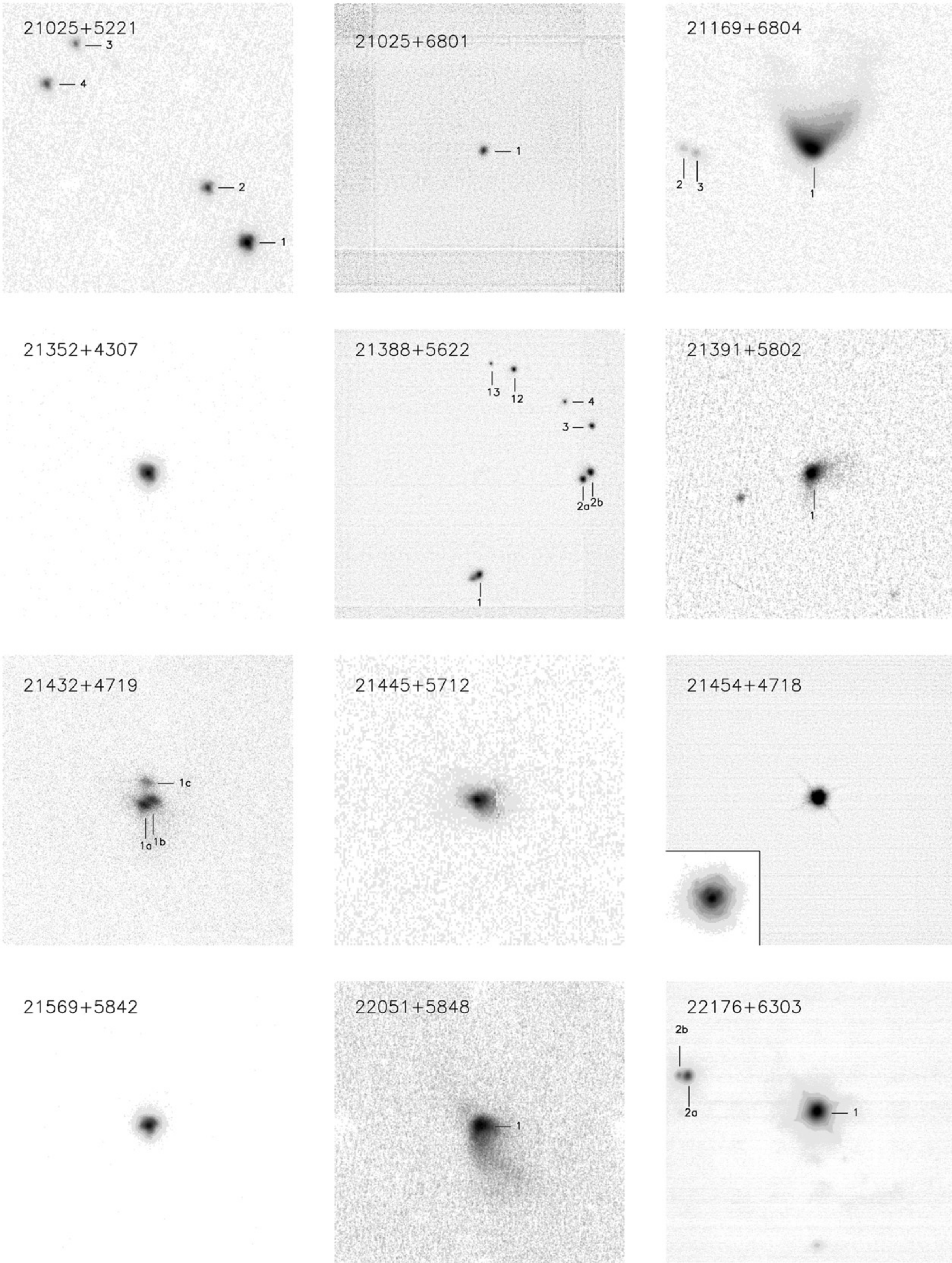

Figure 6. (Continued)

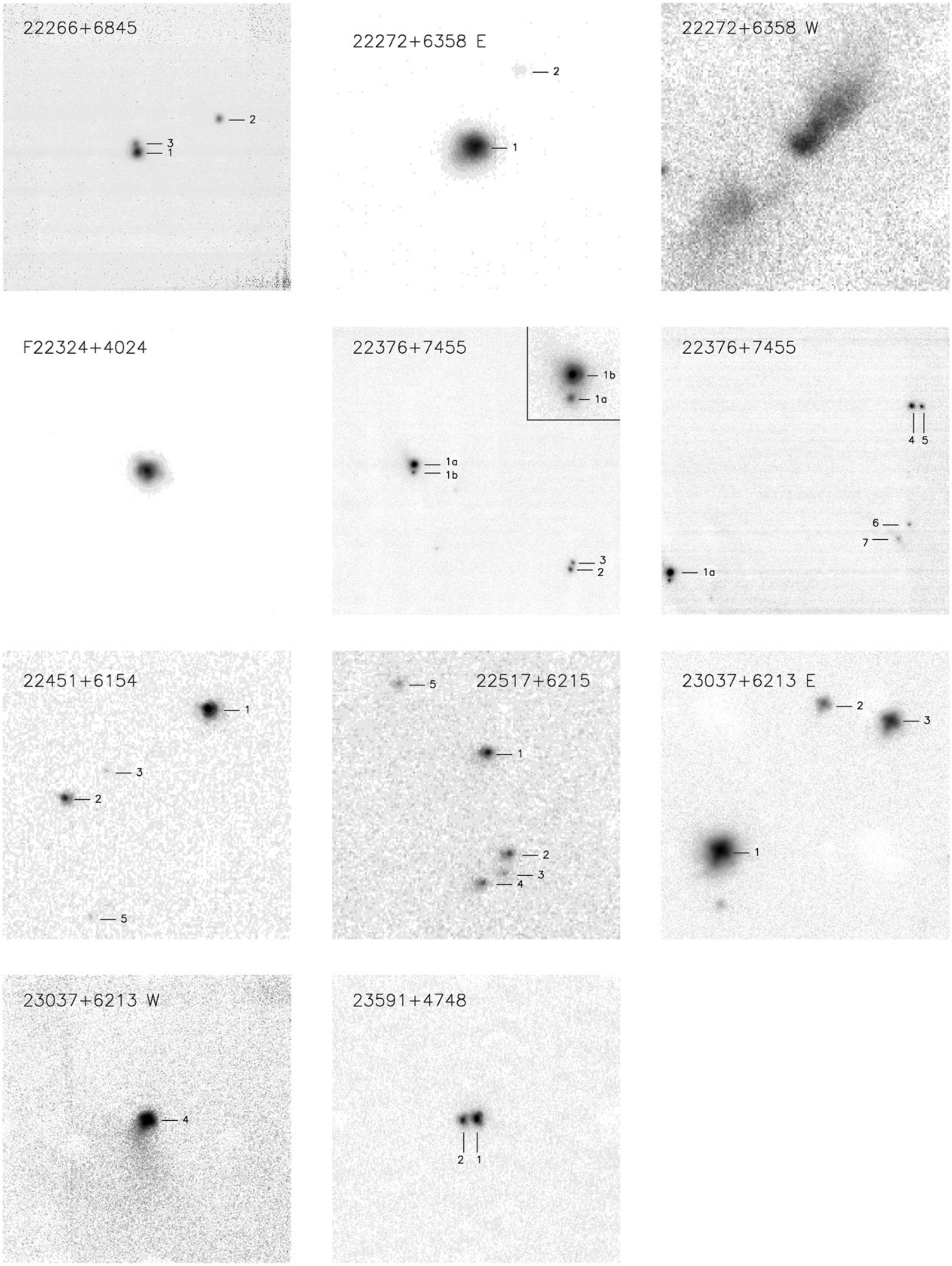

Figure 6. (Continued)

a companion star. PSF fitting and subtraction was done with our L' data only to reveal very close and faint companions. The most successful PSF model was another field star in the same image. Since the image of the field star and target star were taken simultaneously, the PSFs of the two are nearly identical, and thus the field star is an excellent PSF model. However, this method could only be used rarely since the probability of another bright star being in the field of view is quite low. We usually used stars observed just before and just after the target to be subtracted, and combined these two PSFs into a model PSF for the one to be subtracted. The typical peak counts of the residual after PSF subtraction using this method are about 4% of the PSF's peak counts and are typically found about 1 FWHM from the center of the PSF. There were cases where a star had excessive PSF residuals, either from a poor fit or due to scattered light off of circumstellar material at L'. Scattered light was much less of a problem at L' than at K but is still present, especially very close too the star. Excessive PSF residuals affected how close we could detect fake binary companions (described below), and this is reflected in our inner detection limits.

Knowing when companion stars could have been missed is nearly as important as detecting the companions themselves. Our data are less sensitive to close and faint companion stars. Thus, for each target, we needed to determine the closest separation that a companion of a given contrast could have been found so that we could later correct for our incomplete sensitivity to close and faint companions. To do this, we inserted artificial companions at a range of contrasts ($\Delta L' = 1$, 2, 3, and 4 mag fainter than the primary star) into the PSF-subtracted image of each target star, regardless of whether it has a real binary companion. At each contrast level, we inserted 20 artificial companion stars, one at a time, at a known radius but at a random position angle into the PSF-subtracted image. The image of each artificial binary was viewed for 1 s to ensure that we could easily and confidently find the artificial companion. The artificial companion also had to be easy enough to recover so that, if we were examining real data, we would confidently believe that we had found a companion star. Each artificial binary image was followed by an image of blank sky, also for 1 s, because we found that it was too easy to see the artificial companion "jump" around the image if images of artificial binary companions in different locations were viewed consecutively. If the companion could be recovered at least 19 out of 20 times, then the artificial companion would be inserted at a closer separation and the test repeated until the artificial companion could not be reliably recovered 95% of the time. The inner detection limit is determined to be the closest separation where the artificial companion could be reliably detected at least 95% of time. This test was repeated for each of the four contrast levels mentioned above, and for each individual star.

This method has the disadvantage that we know at what separation to expect artificial companions to be found. However, if we placed artificial companion stars at random separations and random position angles, most of the artificial stars would be inserted at a separation either too close to be recovered, or far enough away to be trivially detected. Even in the case where the artificial star is inserted at a random separation, we are most interested in artificial companions in the separation range where it is possible but difficult to detect the artificial companion. The method we used has the advantages that it quickly identifies the inner separation limit, and it uses the same method used for identifying real binary companions. Table 5 lists the binary systems that we identified. Table 6 lists the inner

Table 5
Binary Properties

IRAS	#[a]	$d(pc)$	$\Delta L'$[b]	r ($''$)[c]	P.A.[d]	Discoverer
03220+3035		290	1.30	1.37	200.3	Hodapp (1994)
F03258+3105		220	0.05	0.99	91.5	New
03260+3111	1	290	0.81	0.55	81.7	New
03260+3111	1	290	3.29	3.77	49.2	Haisch et al. (2004)
03331+6256	1	1560	0.05	2.34	212.4	New
04073+3800	1	350	5.18	12.94	28.6	Weintraub (1992)
04108+2803	2	140	0.44	21.64	64.5	Myers et al. (1987)
04113+2758	1	140	0.60	3.97	154.3	Kenyon et al. (1990)
04169+2702	1	140	1.63	0.18	106.6	New
04189+2650	1	140	2.99	0.31	128.9	New
04189+2650	2	140	2.84	19.75	275.7	Mundt et al. (1984)
04191+1523		140	3.27	5.97	305.2	Duchêne et al. (2004)
04223+3700		350	3.56	1.10	85.6	New
04239+2436		140	1.47	0.30	282.7	Reipurth et al. (2000)
04288+2417		140	3.50	2.30	171.4	Cohen & Kuhi (1979)
04325+2402		140	2.63	8.03	351.4	Hartmann et al. (1999)
05155+0707	1	460	2.78	6.58	73.4	Osterloh et al. (1997)
05283−0412	1	470	0.47	4.54	308.8	New
05289−0430E		470	2.64	0.29	346.2	New
05302−0537		470	0.16	0.65	27.4	New
05327−0457	1	450	1.23	0.14	80.3	New
05327−0457	2	450	0.49	2.25	237.1	New
05327−0457	6	450	0.50	3.63	184.7	New
05327−0457	5	450	0.31	2.77	335.4	New
05340−0603	2	470	0.78	0.24	357.3	New
05375−0040	1	470	1.68	6.40	279.0	New
05379−0758	1	480	4.11	0.52	0.7	New
05384−0807	1	480	1.81	0.37	141.5	New
05384−0807	3	480	1.89	0.18	355.3	New
05384−0807	4	480	0.78	0.08	327.5	New
05384−0807	6	480	0.73	0.16	314.4	New
05391−0841	1	480	3.76	0.72	311.7	New
05391−0841	2	480	3.28	5.38	164.3	Chen & Tokunaga (1994)
			0.45	9.49	333.8	Chen & Tokunaga (1994)
05404−0948		480	2.49	3.59	204.9	New
05404−0948		480	2.36	0.16	135.3	New
05417+0907		465	0.86	1.21	209.7	New
05427−0116		470	1.32	0.81	351.6	New
05548−0935	2	470	0.87	4.22	22.9	New
05548−0935	2	470	0.37	10.55	222.5	New
05555−1405	1	470	0.08	5.80	177.6	New
05555−1405	1	470	1.55	0.21	115.2	New
05564−1329		470	0.68	4.48	252.0	New
05598−0906	1	470	4.23	0.93	98.8	New
05598−0906	5	470	0.90	0.44	177.8	New
05598−0906	7	470	3.45	0.85	15.3	New
06249−0953		830	0.33	2.30	262.6	New
06297+1021E		830	4.94	5.50	341.8	New
06382+1017	1	800	2.46	1.82	336.6	Piché et al. (1995)
06382+1017	1	800	1.85	0.21	16.1	New
07025−1204	2	1150	0.43	0.34	330.4	New
07025−1204	2	1150	1.56	2.37	142.7	New
07025−1204	4	1150	3.58	1.49	356.6	New
07025−1204	4	1150	4.45	0.62	355.8	New
07028−1100	1	1150	3.94	2.37	48.1	New
16288−2450E		160	2.85	0.62	199.8	New
16288−2450W		160	1.95	2.98	241.0	Hodapp (1994)
16288−2450W		160	5.88	14.72	127.4	New
17369−1945	1	160	0.96	1.50	78.4	New
17369−1945	1	160	2.68	1.59	30.5	New
17369−1945	1	160	1.83	3.48	356.6	New
18270−0153	1	none	4.21	5.68	63.7	New
18270−0153	4	none	2.19	1.48	70.6	New
18270−0153	6	none	1.25	1.93	313.8	New
18273+0034	2	310	2.51	9.53	302.8	New
18278−0212	1	600	0.15	4.47	328.0	New

Table 5
(Continued)

IRAS	#[a]	$d(pc)$	$\Delta L'$[b]	r ($''$)[c]	P.A.[d]	Discoverer
18340−0116	1	none	1.47	2.83	32.3	New
18340−0116	1	none	1.43	7.90	36.8	New
18383+0059	3	none	0.39	2.15	280.8	New
18383+0059	1	none	1.85	0.18	141.3	New
19247+2238	1	none	0.69	1.57	143.7	New
19247+2238	3	none	0.97	0.24	6.3	New
21004+7811		300	2.52	2.47	235.3	New
21025+5221	1	none	1.41	4.72	35.7	New
21025+5221	3	none	0.50	3.47	324.3	New
21169+6804	1	450	4.10	8.97	92.0	Yun & Clemens (1994)
21169+6804	3	450	0.32	1.01	68.5	New
21388+5622	2	750	0.63	0.71	133.2	New
21388+5622	3	750	1.34	2.49	47.6	New
21432+4719	1	900	0.04	0.66	119.5	New
21432+4719	1	900	1.17	1.52	13.3	New
22266+6845	1	200	2.18	6.95	292.2	New
22266+6845	1	200	2.16	0.62	10.0	New
22272+6358E	1	950	5.08	6.19	330.2	New
22376+7455	1	330	2.22	0.54	176.3	New
22376+7455	2	330	0.49	0.49	340.0	New
22376+7455	6	330	0.16	1.24	142.6	New
23037+6213	3	700	1.87	4.83	75.5	New
23591+4748		800	0.93	0.98	96.7	New

Notes.
[a] The number of the primary star in the finder charts if there is more than one primary object per *IRAS* source.
[b] The L' magnitude difference between the primary and secondary stars.
[c] The angular separation from the primary to the secondary star.
[d] The position angle of the secondary star.
(This table is also available in a machine-readable form in the online journal)

detection limit for each star at four contrast levels, as well as the outer companion acceptance limit (described below) at each of the four contrast levels.

4.3. Outer Detection Limit

The purpose of imposing an outer separation limit, beyond which no object would be considered as a companion, is to ensure that all candidate companions are likely to be gravitationally bound companions to the primary star and to help eliminate background star contamination. Duchêne et al. (2004) used an outer limit of $10''$(1400 AU at the distance of their targets). They argue that this outer limit is much smaller than the typical size of a typical core in the regions they observed; thus these binaries are likely to have formed from the collapse of the same core or filament. Reipurth & Zinnecker (1993) used an outer limit of 1800 AU. They argue that the typical star-to-star separation in a low-density star-forming region is ∼20,000 AU, and is ∼10,000 AU in a high-density region such as the Trapezium cluster. As such, 1800 AU is an order of magnitude smaller than the typical star-to-star separations for the regions that the targets observed by Reipurth & Zinnecker (1993) are in, and thus they argue that these companions are likely to be gravitationally bound.

There are a handful of well-known common proper motion binary stars with very wide separations that are believed to be gravitationally bound. Perhaps the first star to be recognized as a real binary (versus an optical double) is β Capricorni (Mitchell 1767), which has a projected separation of 9400 AU. ϵ Lyrae 1 and 2 have a common proper motion and a projected separation of 13,000 AU (Burnham 1978). While it is rare for a companion to have a separation in excess of 2000 AU, it is possible for such widely separated stars to be gravitationally bound. Furthermore, the mean velocity dispersion of CO gas in the Taurus clouds is 1.4 km s^{-1}, and the observed radial velocity dispersion of Class I protostars is consistent with this value (Covey et al. 2006). At this velocity, it would take 1.7×10^4 years, or roughly the Class 0 life time, to drift 5000 AU. Thus, close but gravitationally unbound stars should be more than 5000 AU apart by the time they are visible in the near-IR as Class I YSOs. We accept companions with projected separation as great as 5000 AU in order to include widely separated companions with confidence that they are likely to be gravitationally bound.

The probability of background star contamination within a projected separation of 5000 AU could exceed 5%, which we consider unacceptably high. This is particularly true in regions near the Galactic center. We used star counts in our L' data to estimate the probability of contamination for each target. We counted all stars in our L' images with near-IR colors consistent with field stars. Since there are many fields with no apparent field stars, we grouped these fields into seven regions of Galactic longitude and latitude to improve the count statistics. Having also derived the L' apparent magnitude distribution for all stars in all fields, we used the star counts in a given region to estimate the density of field stars less than $L' = 4$ mag fainter than each of the primary stars in that region. We used this density and Equation (1) from Correia et al. (2006) to estimate the radius from the star where the probability of contamination exceeds 5%. This angular radius is

$$\theta = \sqrt{-\ln(1-P)/\pi\Sigma} \tag{1}$$

where θ is the angular radius with the probability of contamination P (in our case, $P = 0.05$), and Σ is the surface density of field stars in that region of Galactic longitude and latitude that are less than $L' = 4$ mag fainter than the YSO in question. If the 5% contamination radius has a projected radius less than 5000 AU, then the contamination limited radius was used as the outer limit for accepting companions. Otherwise, 5000 AU was used. Although the maximum chance of contamination is 5%, the average chance of contamination within the adopted outer separation limit is 3.0%. Thus we expect there are ∼6 (189 × 0.03) stars identified as binary companions that are background contamination stars. We note that there are a number of fields where the stellar density is so high that we can not confidently identify which object in the field, if any, is the near-IR counterpart to the *IRAS* source. These targets were thrown out and not considered as having been observed.

4.4. Color Selection Criteria

The goal of observing our targets in three bands was to use the location of each star observed (target, candidate companion, or background star) on an $H-K$ versus $K-L'$ color–color diagram to minimize the chance of background star contamination. The $H-K$ versus $K-L$ color–color diagram is divided into three main regions: a region of forbidden colors to the left of the reddening vector from the main sequence, a region of colors consistent with a reddened T Tauri star, and a region of colors consistent with a protostar having an IR excess greater than a T Tauri star (the region for reddened main-sequence stars is very narrow). The colors of unreddened T Tauri stars (in the CIT photometric system, not in the MKO system) were adopted from Meyer et al. (1997). The direction of the reddening vector was

Table 6
Binary Detection Limits

IRAS	#[c]	d (pc)	Inner detection limits ($''$)[a]				Outer detection limits ($''$)[b]			
			$\Delta L' = 1$	$\Delta L' = 2$	$\Delta L' = 3$	$\Delta L' = 4$	$\Delta L' = 1$	$\Delta L' = 2$	$\Delta L' = 3$	$\Delta L' = 4$
00465+5028		800	0.25	0.30	0.72	999.0	6.25	6.25	6.25	6.25
01166+6635		249	0.26	0.26	0.41	0.70	10.53	6.75	5.35	5.05
02086+7600		180	0.39	999.0	999.0	999.0	27.78	20.19	16.01	15.13
03220+3035		290	0.28	0.30	0.42	0.72	17.24	17.24	17.24	17.24
03225+3034		290	0.27	999.0	999.0	999.0	17.24	17.24	17.24	17.24
F03258+3105		220	0.27	0.27	0.27	999.0	22.73	22.73	22.73	20.53
03260+3111	1	290	0.30	0.33	0.72	0.96	17.24	17.24	17.24	17.24
03260+3111	10	290	0.27	0.48	0.66	0.84	17.24	17.24	17.24	17.24
03271+3013		290	0.30	999.0	999.0	999.0	17.24	17.24	17.24	17.24
03301+3111		350	0.36	0.60	0.84	1.08	14.29	14.29	14.29	14.29

Notes.
[a] The closest distance from the primary star that a fake companion star of the stated magnitude difference could be detected. If inner detection limit is 999, then a companion of that contrast cannot be detected at any separation.
[b] The farthest that a binary companion could be accepted. This is limited by our 5000 AU separation limit or the 5% contamination criterion.
[c] The number of the primary star in the finder charts if there is more than one primary object per *IRAS* source.
(This table is available in its entirety in a machine-readable form in the online journal. A portion is shown here for guidance regarding its form and content)

derived from interstellar extinction values (assuming $R = 5$, characteristic of dense clouds) taken from Mathis (2000). Using these values, the $H - K$ reddening is 0.079 per magnitude of $A(V)$ extinction, and the $K - L$ (not MKO L') reddening is 0.066 per magnitude of $A(V)$ extinction. Thus, the reddening vector has a slope of 1.20 on the $H-K$ versus $K-L$ color–color diagram.

We excluded those stars whose colors are consistent with a reddened or unreddened main-sequence star or with forbidden colors, with due caution. The colors of a close companion star are difficult to determine accurately due to the proximity of the brighter primary star. Photometric errors and variability affect the measured colors. Reflection nebulosity can strongly affect the observed colors of a star, especially at the H and K bands. Nebulosity makes the star appear bluer, and may not be spatially resolved. The colors of a protostar can range from the forbidden region (if the near-IR flux is dominated by scattered light) to the region characteristic of objects with a strong IR excess. As such, the color information had to be used with other selection criteria, such as the proximity to the IRAS position and the presence of a spatially resolved reflection nebula, to decide if a star is likely to be an embedded YSO or background contamination. Star counts were used along with colors since colors alone are not sufficient to mitigate the chance of background star contamination.

4.5. Discovery Space

Choosing which candidate companion stars would be retained for further consideration depended on several factors. Stars with $H - K$ and $K - L'$ colors near 0 are likely to be foreground stars and were excluded. An optical or IR reflection nebula is a clear sign that the object in question is physically associated with the cloud. Accurate colors often could not be determined for very close companions. Given the very low probability of contamination at such close separations, these candidate companions were kept.

Figure 7 shows the range of separations and contrasts over which we actually found binary companions. The number of companions versus log(separation/1$''$) is relatively constant. When plotted against linear separation (arcseconds), most of the binaries have separations less than 3$''$. Also, for most of the range of separations, we are not less sensitive to fainter companions than brighter ones. It is only within a few times the FWHM (typically less than 1$''$) that we are less sensitive to faint companions due to the glare of the primary star and, in a few cases, nebulosity. At wider separations, we can be less sensitive to faint companions since our data are not always deep enough to detect companions $\Delta L' = 4$ fainter than the primary star.

5. BINARY COLOR DIFFERENCES

A large number of our binary systems have very different colors between the two components, a situation analogous to the infrared companions of T Tauri stars. The prototypical case, T Tauri N and S, differ in their $H - K$ colors by 1.39 mag and in their $K - L$ colors by 2.0 mag (Ghez et al. 1991). Zinnecker & Wilking (1992) estimated that roughly 10% of T Tauri binary stars have an IR companion.

To find Class I analogs to T Tauri IR companions, we considered the difference in $H - K$ and $K - L'$ colors between the components of binary systems. This examination is limited to objects for which we have photometric data and where the binary is sufficiently well resolved that we have accurate photometry on each component. We were able to derive 49 $H - K$ color differences and 59 $K - L'$ color differences. The color difference distributions are shown in Figure 8. Both color difference distributions are centered near a color difference of 0, with the median $\Delta(H - K) = 0.016$, and the median $\Delta(K - L') = 0.245$. The $\Delta(K - L')$ distribution is slightly wider than the distribution of $\Delta(H - K)$, the standard deviations being 1.11 and 0.89, respectively. Thus, there is no statistically significant preference toward the primary star (defined as the brightest star at L') or the companion being redder. We find that $6/59$ $\left(10.2\%^{+5.6\%}_{-3.9\%}\right)$ of our Class I binaries have a $K - L'$ color difference more extreme than the T Tauri system, and $9/56$ $\left(16.1\%^{+6.4\%}_{-5.0\%}\right)$ have a $H - K$ color difference more extreme than the T Tauri system, including seven targets where we have a lower limit on the H magnitude

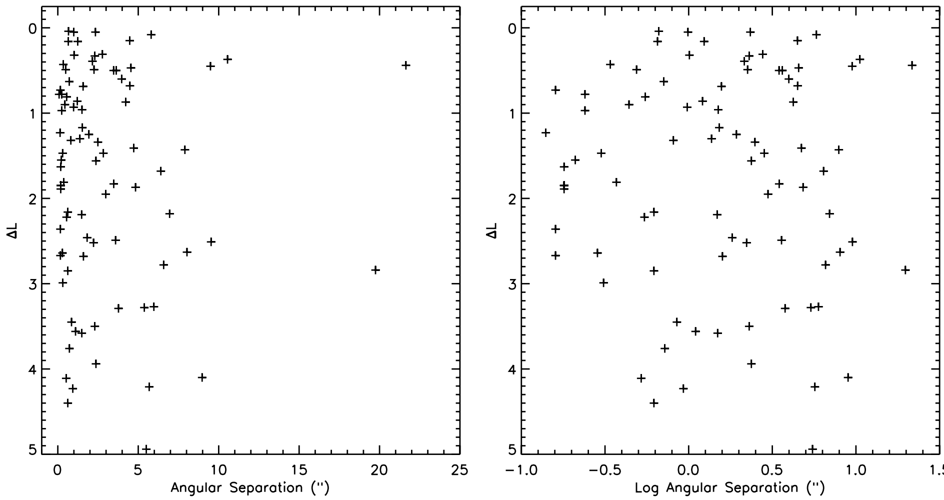

Figure 7. Discovery space. These figures show the contrast of Class I binary companions versus angular separation (left) and versus log(angular separation/1″). We only appear to be losing binary companions at a contrast higher than $\Delta L' = 3$ and closer than 0″.5.

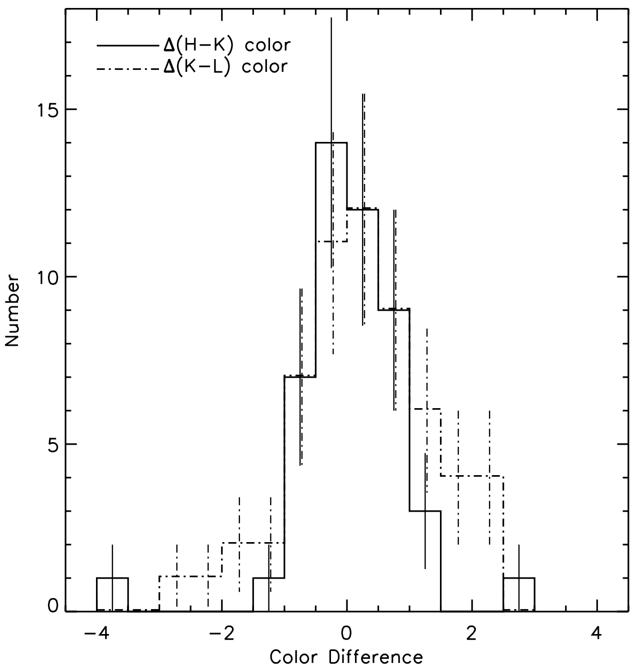

Figure 8. The $H - K$ and $K - L'$ color difference distributions. Both distributions are centered near a color difference of 0. 16% of $H - K$ color differences and 10% of $K - L'$ color differences have color differences greater than the T Tauri system. This percentage of Class I binaries with strong color differences is similar to the fraction of T Tauri stars with IR companions. This figure does not include objects where we only have a lower limit on the H-band magnitude.

of one of the components. We note that only scattered light was detected at the H and/or K band for several targets, which naturally affects the observed colors. We find that protostellar analogs to T Tauri IR companions are quite rare. These values are consistent with the fraction of T Tauri stars that have an IR companion, suggesting a similar origin.

6. SUMMARY

We have presented the results of a near-IR survey for binary stars in a new sample of nearby Class I protostars. The purpose of this paper is to make our observations available to the community, to stimulate follow-up research on these protostars, and to present data on protostellar binary stars for detailed statistical analysis that is presented in Paper II. This survey is distinguished by its well-determined sample properties, large sample size, and choice of using L' observations to identify protostellar binary companions. We found 89 companion stars to 189 primary stars, 78 of which are within a projected separation of 5000 AU and have a contrast less than $\Delta L' = 4$ mag. We have empirically determined our companion detection limits to account for our incomplete sensitivity to binary companions. Separation and contrast limits were chosen to minimize the chance of background star contamination. The average chance of background star contamination is 3.0%, and we expect there are six stars identified as binary companions that are contamination. Near-IR colors were used to identify contaminant stars and we showed that infrared companions are as rare among Class I YSOs as they are among T Tauri stars.

We thank the referee for helpful comments. This research has made use of the SIMBAD database, operated at CDS, Strasbourg, France. This research has made use of NASA's Astrophysics Data System. This publication makes use of data products from the Two Micron All Sky Survey, which is a joint project of the University of Massachusetts and the Infrared Processing and Analysis Center/California Institute of Technology, funded by the National Aeronautics and Space Administration and the National Science Foundation. This research was supported by an appointment to the NASA Postdoctoral Program at the Ames Research Center, administered by the Oak Ridge Associated Universities through a contract with NASA.

REFERENCES

André, P., et al. 1999, ApJ, 513, 57
Aspin, C., & Sandell, G. 1997, MNRAS, 289, 1
Bachiller, R., et al. 2001, A&A, 372, 899
Battinelli, P., & Capuzzo-Dolcetta, R. 1991, MNRAS, 249, 76
Birkmann, S., et al. 2006, ApJ, 637, 380
Bourke, T. 2001, ApJ, 554, 91
Burnham, R. 1978, Burnham's Celestial Handbook (New York: Dover)
Cambresy, L., et al. 1998, A&A, 338, 977

Chen, H., & Tokunaga, A. 1994, ApJS, 90, 149
Clark, J., & Porter, J. 2004, A&A, 427, 839
Cohen, M., & Kuhi, L. 1979, ApJS, 41, 743
Cohen, M. 1980, AJ, 85, 29
Connelley, M., Reipurth, B., & Tokunaga, A. 2007, AJ, 133, 1528
Connelley, M., Reipurth, B., & Tokunaga, A. 2008, AJ, 135, 2526 (Paper II)
Correia, S., Zinnecker, H., Ratzka, T., & Sterzik, M. 2006, A&A, 459, 909
Covey, K., Greene, T., Doppmann, G., & Lada, C. 2006, AJ, 131, 512
Davis, C., et al. 2001, MNRAS, 326, 524
Duchêne, G., Bouvier, J., Bontemps, S., André, P., & Motte, F. 2004, A&A, 427, 651
Duchêne, G., Delgado Donate, E., Haisch, K., Loinard, L., & Rodríguez, L. 2007, in Protostars and Planets V, ed. B. Reipurth, D. Jewitt, & K. Keil (Tucson, AZ: Univ. Arizona Press), 379
Duquennoy, A., & Mayor, M. 1991, A&A, 248, 485
Ghez, A., Neugebauer, G., Gorham, P., Haniff, C., Kulkarni, S., Matthews, K., Koresko, C., & Beckwith, S. 1991, AJ, 102, 2066
Gregorio-Hetem, J., et al. 1988, A&AS, 76, 347
Guetter, H. 1992, AJ, 103, 197
Guetter, H., & Turner, D. 1997, AJ, 113, 2116
Hachisuka, K., et al. 2006, ApJ, 645, 337
Haisch, Jr., K., Greene, T., Barsony, M., & Stahler, S. 2004, AJ, 127, 1747
Hartmann, L., Calvet, N., Allen, L., Chen, H., & Jayawardhana, R. 1999, AJ, 118, 1784
Henning, Th., & Launhardt, R. 1998, A&A, 338, 223
Heyer, M., et al. 1996, ApJ, 464, 175
Hilton, J., & Lahulla, J. 1995, A&AS, 113, 325
Hodapp, K. 1994, ApJS, 94, 615
Hodapp, K., et al. 1996, New Astron., 1, 177
Huard, T., et al. 1999, ApJ, 526, 833
Hughes, J., & Hartigan, P. 1992, AJ, 104, 680
Karr, J., & Martin, P. 2003, ApJ, 595, 900
Kenyon, S., Hartmann, L., Strom, K., & Strom, S. 1990, AJ, 99, 869
Knude, J., & Hog, E. 1998, A&A, 338, 897
Kobayashi, N., et al. 2000, Proc. SPIE 4008, ed. M. Iye, & A. Moorwood, 1056
Krisciunas, K. 1987, PASP, 99, 887
Kun, M., et al. 2001, PASJ, 53, 1063
Lada, C. 1991, in The Physics of Star Formation and Early Stellar Evolution, ed. C. J. Lada, & N. D. Kylafis (Dordrecht: Kluwer), 329
Larson, R. 2001, in IAU Symposium 200: The Formatio of Binary Stars, ed. H. Zinnecker, & R. Mathieu (San Francisco: ASP), 93
Launhardt, R., & Henning, Th. 1997, A&A, 326, 329
Liseau, R., et al. 1992, A&A, 265, 577
Maheswar, G., et al. 2004, MNRAS, 355, 1272
Marco, A., et al. 2001, AJ, 121, 2075
Marraco, H., & Rydgren, A. 1981, AJ, 86, 62
Mathieu, R., Ghez, A., Jensen, E., & Simon, M. 2000, in Protostars and Planets IV, ed. Mannings, Boss, & Russell (Tucson, AZ: Univ. Arizona Press), 703
Mathis, J. 2000, in Allen's Astrophysical Quantities, ed. A. N. Cox (Melville, NY: Springer)
Meyer, M., Calvet, N., & Hillenbrand, L. 1997, AJ, 114, 288
Mikami, T., & Ogura, K. 1994, MNRAS, 270, 199
Mitchell, J. 1767, Phil. Trans. R. Soc., 57, 234
Monet, D., et al. 2003, AJ, 125, 984
Mookerjea, B., et al. 2000, ApJ, 539, 775
Moreira, M., et al. 2000, AJ, 119, 2960
Mundt, R., Büehrke, T., Fried, J., Neckel, T., Sarcander, M., & Stocke, J. 1984, A&A, 140, 17
Murakawa, K., et al. 2004, PASJ, 56, 509
Myers, P., Fuller, G., Mathieu, R., Beichman, C., Benson, P., Schild, R., & Emerson, J. 1987, ApJ, 319, 340
Neri, L., et al. 1993, A&AS, 102, 201
Obayashi, A., et al. 1998, AJ, 115, 2740
Osterloh, M., Henning, Th., & Launhardt, R. 1997, ApJS, 110, 71
Patience, J., Ghez, A., Reid, I., & Matthews, K. 2002, AJ, 123, 1570
Piché, F., Howard, E., & Pipher, J. 1995, MNRAS, 275, 711
Prato, L., et al. 2003, ApJ, 584, 853
Price, S., Egan, M., Carey, S., Mizuno, D., & Kuchar, T. 2001, AJ, 121, 2819
Racine, R. 1968, AJ, 73, 233
Ramsay Howat, S., et al. 2004, SPIE, 5492, 1160
Rayner, J., Toomey, D., Onaka, P., Denault, A., Stahlberger, W., Vacca, W., Cushing, M., & Wang, S. 2003, PASP, 115, 362
Reipurth, B., & Aspin, C. 1997, AJ, 114, 2700
Reipurth, B., et al. 1993, A&A, 273, 221
Reipurth, B. 1999, A General Catalog of HH Objects (http:casa.colorado.edu/hhcat/)
Reipurth, B., & Zinnecker, H. 1993, A&A, 278, 81
Reipurth, B., Yu, K., Heathcote, S., Bally, J., & Rodríguez, L. 2000, AJ, 120, 1449
Sagar, & Joshi 1983, MNRAS, 205, 747
Simons, D., & Tokunaga, A. 2002, PASP, 114, 169
Straizys, V., et al. 1992, BaltA, 1, 149
Sugitani, K., & Ogura, K. 1994, ApJS, 92, 163
Sugitani, K., & Ogura, K. 1995, Ap&SS, 224, 571
Sugitani, K., et al. 1991, ApJS, 77, 59
Tamura, M., et al. 1997, MNRAS, 287, 894
Tokunaga, A., & Simons, D. 2002, PASP, 114, 180
Tokunaga, A., et al. 1998, SPIE, 3354, 512
Vilas-Boas, J., et al. 2000, ApJ, 532, 1038
Weintraub, D. 1992, BAAS, 24, 1141
Wilson, B., et al. 2005, A&A, 430, 523
Wouterloot, J., & Brand, J. 1989, A&AS, 80, 149
Wouterloot, J., & Brand, J. 1999, A&AS, 140, 177
Yun, J., et al. 2001, A&A, 372, 33L
Yun, J., & Clemens, D. 1994, ApJS, 92, 145
Zhang, C., et al. 1988, A&A, 199, 170
Zinnecker, H., & Wilking, B. 1992, in Binaries as Tracers of Stellar Formation, ed. A. Duquennoy, & M. Mayor (Cambridge: Cambridge Univ. Press), 269